Time-dependent fiber bundles with local load sharing

W. I. Newman
Departments of Earth and Space Sciences, Physics and Astronomy, and Mathematics, University of California, Los Angeles, California 90095-1567
and Department of Computer Science and Applied Mathematics, Weizmann Institute of Science, Rehovot 76100, Israel

S. L. Phoenix
Department of Theoretical and Applied Mechanics and Sibley School of Mechanical and Aerospace Engineering, Cornell University, Ithaca, New York 14853

(Received 21 July 2000; revised manuscript received 19 October 2000; published 24 January 2001)

Fiber bundle models, where fibers have random lifetimes depending on their load histories, are useful tools in explaining time-dependent failure in heterogeneous materials. Such models shed light on diverse phenomena such as fatigue in structural materials and earthquakes in geophysical settings. Various asymptotic and approximate theories have been developed for bundles with various geometries and fiber load-sharing mechanisms, but numerical verification has been hampered by severe computational demands in larger bundles. To gain insight at large size scales, interest has returned to idealized fiber bundle models in 1D. Such simplified models typically assume either equal load sharing (ELS) among survivors, or local load sharing (LLS) where a failed fiber redistributes its load onto its two nearest flanking survivors. Such models can often be solved exactly or asymptotically in increasing bundle size, N, yet still capture the essence of failure in real materials. The present work focuses on 1D bundles under LLS. As in previous works, a fiber has failure rate following a power law in its load level with breakdown exponent ρ. Surviving fibers under fixed loads have remaining lifetimes that are independent and exponentially distributed. We develop both new asymptotic theories and new computational algorithms that greatly increase the bundle sizes that can be treated in large replications (e.g., one million fibers in thousands of realizations). In particular we develop an algorithm that adapts several concepts and methods that are well-known among computer scientists, but relatively unknown among physicists, to dramatically increase the computational speed with no attendant loss of accuracy. We consider various regimes of ρ that yield drastically different behavior as N increases. For $1/2 \leqslant \rho \leqslant 1$, ELS and LLS have remarkably similar behavior (they have identical lifetime distributions at $\rho = 1$) with approximate Gaussian bundle lifetime statistics and a finite limiting mean. For $\rho > 1$ this Gaussian behavior also applies to ELS, whereas LLS behavior diverges sharply showing brittle, weakest volume behavior in terms of characteristic elements derived from critical cluster formation. For $0 < \rho < 1/2$, ELS and LLS again behave similarly, but the bundle lifetimes are dominated by a few long-lived fibers, and show characteristics of strongest link, extreme value distributions, which apply exactly to $\rho = 0$.

DOI: 10.1103/PhysRevE.63.021507 PACS number(s): 83.80.Ab, 62.20.Mk, 81.40.Np

I. INTRODUCTION

A. Background

Statistical aspects of fracture processes in heterogeneous materials have received increasing attention over the past two decades, not only because of their richness in physical and mathematical phenomena, but also because of the possibility of designing material microstructures that produce highly reliable components. Such models have also been of interest in geophysical settings to explain earthquake behavior. While much attention has been devoted to static or fast-fracture strength, where material elements are assumed time-independent, models describing creep-rupture and fatigue lifetime are perhaps even more important. In both cases, important issues are flaw character and interactions during breakdown, dispersed versus localized damage evolution, the associated forms of ultimate strength and lifetime distributions (especially lower-tail behavior), and size or scale effects. Building good theoretical models has proven straightforward, but analyzing them has required delving into statistical details of the interaction of various flaw features and failure configurations, which has proven to be deceptively difficult. Behavior is rarely captured by mean field approaches that otherwise work well in studying transport and percolation determined properties.

One approach to modeling such detail has been to develop discrete network or lattice models in various dimensions, where the geometry of the lattice (hexagonal, square, cubic, etc.), the load redistribution from failed to surviving elements, and the probability model for element failure must be specified. Time dependence (including load-history effects) typically enters through the element failure model, but it also can appear through the load redistribution model. The resulting breakdown behavior, whether localized or dispersed, is strongly influenced by the variability built into the element failure model and the intensity of stress concentration occurring in load redistribution. Subtle changes in parameter values can lead to dramatic changes in breakdown statistics.

The earliest and simplest models appearing in the literature are fiber bundle models. In the case of fast fracture, the classic work is that of Daniels [1] on the strength of simple fiber bundles under equal load sharing (ELS) among non-

failed fibers. A key result from a highly nontrivial analysis is that the strength is asymptotically Gaussian with variability decreasing inversely as the square-root of the number of fibers. More realistic material failure models have often assumed a chain-of-bundles structure [2–4], where bundle length is a characteristic length of fiber load transfer and material strength is determined by the weakest bundle. The resulting strength follows a double-exponential, extreme value distribution associated with Gaussian distributed links.

In the case of time-dependent breakdown, early work on the lifetime of simple fiber bundles under ELS and under steady load was carried out by Coleman [5–7], with subsequent generalizations by Phoenix [8,9]. Corresponding chain-of-bundles versions were also developed [3,6]. The resulting lifetime distributions are similar in form to the static case (with time replacing stress). Though analytically tractable, these dispersed failure ''mean field'' models are more applicable to the strength of weakly bonded, fibrous materials than to tightly bonded materials with elastic fiber load transfer.

Study of the failure of fiber-reinforced composites with strong, well-bonded, elastic matrices has led to another branch of network models, where the load sharing is more localized [10–17], though still within a chain-of-bundles framework. In the case of static strength [10–14], fiber elements are often assumed to follow a Weibull distribution [18], but failed elements are assumed to redistribute their loads locally onto nearby unfailed neighbors, increasing their probabilities of failure and thus the likelihood of a catastrophic cascade. Rendering these models analytically tractable has required highly idealized assumptions in the form of ''load-sharing rules'' on the local fiber load redistribution mechanism. One such model, called local load sharing (LLS), assumes that the loads of failed fibers are shifted in equal portions onto the nearest flanking survivors. For planar versions under LLS with one-dimensional bundle structure, various recursive [13,14] and asymptotic methods [12] have been used with success in the case of static strength. Versions with time-dependent breakdown of fibers have also been developed [13–17]. A more realistic form of localized load-sharing is based on shear-lag models after Hedgepeth [19–21], and is less severe than LLS with some load shifted to more distant neighbors. Recent progress on static strength versions of such models is summarized in a review article by Phoenix and Beyerlein [22].

Network or lattice models of material failure have also received attention in the statistical physics literature, particularly in connection to percolation theory. Because of its strong relationship to mechanical failure, conductivity breakdown in random fuse networks has been studied extensively [23–26]. Such models often consider a planar, square lattice of finite size where the conducting elements are initially fuses with probability p or insulators with probability $q=1-p$, assumptions typical of percolation models. The fuses initially have identical breakdown voltage v_0, and thus, the distribution for element strength is simple and discrete. A voltage gradient is applied along one axis, and calculation of the currents in all the intact fuses is done through numerical solution of Kirchhoff's laws with the resulting localized load sharing being quite similar to the shear-lag models [27]. The strength of the lattice is the largest voltage gradient that the network can sustain before transverse propagation by a wandering cracklike cluster of burnt fuses.

Despite their simplicity and knowledge from percolation theory, these networks have proven to be deceptively difficult to analyze. Monte Carlo simulations on sample fuse networks have been carried out [23–25] to empirically determine the distributions of the critical voltage gradient (strength) that generates a catastrophic cluster. Because of the computational demands, results have been generated only for relatively small lattices up to about 200×200. Nevertheless the critical voltage gradient was seen to decrease inversely as a power of the logarithm of the network size with no apparent positive lower bound.

To explain this size dependence and observed shape of the breakdown voltage distributions, Duxbury and coworkers [24,25] considered the effects of defect clusters in a large lattice in the form of isolated contiguous transverse rows of missing fuse elements, focusing on the current enhancement at the row tips. Considering the statistics of the largest critical defect cluster, namely a transverse slit or ''crack,'' they appealed to the statistical theory of extremes, and determined approximately the distribution function for the normalized breakdown voltage for small q. They obtained a particular double exponential form with dependence on network size. Their results were supported by Monte Carlo simulations on networks up to 200×200 in size [24].

In elastic spring networks with element breakdown structure analogous to the random fuse networks above, the general size scalings and distributional forms above have not always been apparent from simulations [28]. Various continuous distributions for element strength have also been used [28]. Some of these forms appeared to yield scalings similar to those in percolation, rather than as described above for the random fuse networks. Hansen *et al.* [29] argued that, for p above the percolation threshold, rescaling through a renormalization argument leads to the disappearance of disorder as the effective value of p, defined at a given scale converges to unity as the network scale grows large. Thus such models were thought to be asymptotically equivalent to a disorderless system with a finite average strength in an infinite lattice limit, much like ELS fiber bundle models. Perhaps the main origin of controversy over the particular form of the size scaling is that simulations covering many orders of magnitude in sample dimensions are necessary to arrive at definitive conclusions. In most cases, such sizes have been inaccessible by Monte Carlo simulation alone as lattices approaching 500×500 in size have rapidly become too demanding computationally. Also, subtle dependencies on the form of the distribution for element strength were not fully understood. Both are important issues in the present paper.

Regardless of their viewpoints, many investigators have turned to rigorous study of idealized, one-dimensional models [30–34] in an attempt to put approximate analyses and interpretations from simulations of more complex networks on firmer ground. In the case of static strength, such models, which are often variations on the LLS models of Harlow and

Phoenix [10,11,30], are analytically solvable, rich in behavior, and qualitatively show many features seen in simulations. In most cases, results in LLS fiber bundle models support the logarithmic size scaling mentioned above. Generally, such results depend on the load-sharing scheme (LLS versus ELS) as well as on the assumed form of the distribution for element failure. Asymptotic analysis coupled to Monte Carlo simulation has led to improved forms of material strength distributions in recent work [22,35,36].

In localized load-sharing settings involving time-dependent breakdown of elements, some early work on lattice failure was performed by Gotlib *et al.* [37,38]. Curtin and Scher [39–42] also developed such models, and by decreasing the value of the power-law breakdown exponent, ρ, they uncovered transitions from logarithmic scaling to global percolationlike scaling where the lifetime had a finite limit in network size. Interesting power-law behavior has been observed by Hansen *et al.* [43], and Roux *et al.* [44] have recorded some insights into the subtleties of such problems.

Subtle scalings and transitions have also been noticed in fiber bundle models with hierarchical load-sharing, as discussed in Newman *et al.* [45–49]. Much of the motivation in these models emerged from the need to understand the statistics of time sequences and magnitudes of earthquakes. Yamashita and Knopoff (YK) [50] used a deterministic 2D, antiplane continuum mechanics model of stress corrosion/subcritical crack growth and fusion to simulate earthquake foreshock behavior. The continuum model corresponds to the LLS fiber bundle abstraction. The subcritical crack growth rate model corresponds to the power-law breakdown model for fiber elements. Experimentally the power-law exponent ρ is very large, with exponents ranging from 10 to 170 for rocks under Mode I deformation [51]. The large values of ρ suggest perhaps that exponential growth laws should be preferred over power laws; exponential growth rates are usually considered indicative of activation processes and are suggestive of the importance of water in earthquake faults as a corrosive agent in the earthquake process [52], a point of view corroborated by the fact that water is an excellent solvent of the silicate bond in SiO_2. Despite this connection, YK [50] used the power-law form with very large ρ for its computational advantages, as do we. As Phoenix and Tierney [16] have shown, however, the power law also has a firm interpretation as a model for bond failure under stress due to activation processes, whereby the exponent ρ is inversely proportional to absolute temperature.

Because of the continuum nature of the YK model, the stress redistribution law has long range behavior that falls off in distance x as $x^{-1/2}$ for isolated fractures and in a more complex manner for stress fields in the gaps between closely spaced cracks. This load-sharing behavior is much more in line with that seen in the elastic lattices studied by Curtin and coworkers [39–42], than in the LLS bundle model. This suggests that the 2D system should have properties intermediate between the LLS and ELS bundles we study. The numerical results of YK [50] indicate that their system displays a critical point behavior shortly before complete failure and, hence, that interaction among cracks is vitally important. This suggests that system lifetimes should not be gauged by the duration of fracture activity when the population of cracks is dilute; rather the precursory behavior should be scaled relative to the time of failure of the entire system. To some extent this is confirmed in the work of Curtin and coworkers [41,42]. What is also seen, however, is that the effect of interactions depends strongly on the value of the breakdown exponent ρ and the size of the system. Small systems show dispersed ELS-like behavior regardless of the value of ρ. For larger systems, however, divergence from ELS-like behavior eventually occurs for $\rho \geqslant 2$ as interactions play a more subdued role and failure becomes dominated by a single growing crack. The goal of the current paper is to shed further light on these issues.

B. Overview of paper and main results

In this paper we study in detail the one-dimensional bundle model of time-dependent failure under LLS. The probability model for fiber element breakdown is a power-law hazard rate model in terms of an exponent ρ and with exponential lifetime features under fixed load. Versions of this fiber breakdown model have been used in many previous works [7–9,13–17,37–44,46,47].

In Sec. II we describe the basic bundle model, ELS and LLS load-sharing assumptions, and the fiber lifetime model. In Sec. III we discuss theory for ELS for $0<\rho$ because it plays a key role in understanding the behavior of LLS for $0<\rho\leqslant 1$. We discuss the special case $\rho=1$ where ELS and LLS have the same lifetime distributions, though different tendencies of clustering of failed fibers. In the upper end of this regime, $1/2<\rho\leqslant 1$, we give results where the distribution for bundle lifetime is asymptotically Gaussian with known mean and variance.

In Sec. IV we discuss LLS theory. We consider first the case $\rho>1$ where the asymptotic analysis relies on ρ being large. Unlike in ELS, we find brittlelike behavior, cluster nucleation, and growth of an eventual catastrophic crack. We derive the asymptotic distribution for lifetime in terms of a characteristic distribution function, $W(t)$, used in a weakest local volume representation. We also consider failure rate behavior for $0<\rho<1$ making the connection to ELS. Results for the degenerate case $\rho=0$ are discussed where lifetime is governed by the the largest of the fiber lifetimes, and the associated extreme value theory applies. We investigate the extent to which these results, with minor modifications, might apply to the case $0<\rho\ll 1/2$. In many material settings, the important regime is $\rho>1$, but as mentioned earlier, ρ may vary inversely with absolute temperature. Many materials such as silicon nitride ceramics show a ductile to brittle transition at high temperature, and the transitional behavior we uncover at $\rho=1$ exhibits this feature.

In Sec. V we present a comparison of LLS (and ELS) theory to Monte Carlo simulation results for LLS bundles of up to one million fibers in replications greater than 1000. Favorable comparisons are obtained between analytic theory and computational experiment. Section VI concludes with a discussion of some extensions and connections to earlier work.

We defer to the Appendix a discussion of the computational algorithms developed for simulations of bundle failure in kilo-replications of megasize bundles. Our ability to perform the necessary Monte Carlo simulations is the direct outcome of these advances. Readers not concerned with the ability to perform such simulations can omit the Appendix, while those who wish to develop this capability will find this Appendix and its associated reference to be indispensable. In particular, we discuss the difficulties in keeping track of the effects of load history on each fiber, determining on which fibers to place the load shed by a fiber that has just failed, and determining the next fiber to fail in the sequence as well as its failure time. By using pointer arrays and a special-purpose adaptation of merge-sort algorithms in identifying and prioritizing failures, we are able to reduce the two tasks that would have required $\mathcal{O}(N^2)$ operations to $\mathcal{O}(N)$ and $\mathcal{O}(N \ln N)$ operations, respectively.

II. MODEL ASSUMPTIONS

A. Bundle geometry and load sharing rules

We consider a 1D fiber bundle in the form of a linear array of N fiber elements numbered from 1 to N from the left. We apply a positive fixed load L to the bundle on a per fiber basis; that is, initially each fiber is intact and carries load L. As time passes, fibers break leaving an array of failed and surviving fibers. Surviving fibers in an array share load according to a load-sharing rule and we will consider two particular rules.

The first rule is called local load sharing (LLS). In this rule there are three types of survivors: interior survivors, boundary survivors, and a sole survivor. An interior survivor has at least one other survivor somewhere to its left and one other somewhere to its right. A boundary survivor has no survivors on one side (though possibly some failures), but at least one survivor somewhere on its other side. A sole survivor is the only survivor in the bundle. For an interior fiber adjacent to r contiguous failed fibers counting on both its left and right, its load concentration factor, K_r, follows

$$K_r = 1 + \frac{r}{2}, \tag{2.1}$$

where we also take $K_0 = 1$. This means that its actual load is $K_r L$. On the other hand a boundary fiber has load concentration factor $K_{r,b}$, which follows

$$K_{r,b} = 1 + \frac{r}{2} + \frac{b}{2}, \tag{2.2}$$

where b is the number of adjacent broken fibers between it and the boundary and r is as defined before (including also the b fibers). A sole survivor has load concentration N. An alternative view of the rule is that a failed fiber shifts half of its load to the closest survivor on its left and half to the closest survivor on its right, unless there is no such survivor on one side in which case all its load goes to the survivor on the other.

The second rule is called equal load sharing (ELS). In this rule all nonfailed fibers in the bundle share the applied bundle load equally and all failed fibers support no load. Thus if j out of N fibers have failed, the surviving fibers each have load concentration factor

$$K_j^{\mathrm{ELS}} = \frac{N}{N-j}, \quad j = 0,1,2,\ldots,N-1. \tag{2.3}$$

B. Stochastic fiber lifetime model

Fiber elements are assumed statistically identical and independent under a given load history, and the lifetime distribution for a fiber element in terms of its load history, $\ell(t), t \geq 0$, follows

$$F(t;\ell(\cdot)) = 1 - \exp\left\{ -\Psi\left(\int_0^t \kappa[\ell(s)]\,ds \right) \right\}, \tag{2.4}$$

where $\kappa(x)$, $x \geq 0$ is called the breakdown rule and $\Psi(x)$, $x \geq 0$ is called the hazard function. In the present case, we assume the power-law breakdown rule

$$\kappa(x) = x^{\rho}, \tag{2.5}$$

with exponent $\rho \geq 0$, and the Weibull hazard function

$$\Psi(x) = x^{\beta}, \tag{2.6}$$

with Weibull exponent $\beta \geq 0$, where we take $\beta = 1$. When a fiber is under fixed load

$$\ell(t) = L > 0, \tag{2.7}$$

its lifetime distribution is the Weibull distribution

$$F(t;L) = 1 - \exp[-(t/t_L)^{\beta}], \tag{2.8}$$

where $t_L = L^{-\rho}$, but by taking $\beta = 1$, as we are doing, this distribution is actually an exponential distribution with mean and standard deviation both t_L.

In the fiber bundle model we have conveniently taken any scale constants in the breakdown rule or hazard function as unity. Any scale constants that do arise in practice can be absorbed into normalizing load and time parameters. Henceforth we will think of both the load variable L and time variable t as dimensionless.

Taking $\beta = 1$ renders a fiber memoryless, thus simplifying the model. That is, its remaining lifetime given survival to time t is independent of its load history up to time t, and under its current fixed load is also exponentially distributed as though it were new. In Monte Carlo simulations of this type of problem, unlike the common approach of small incremental time steps based only on the current configuration of failed fibers and surviving fiber loads, our simulation algorithm will not use this memoryless property, and thus, can be used in the general case $\beta \neq 1$. Our approach can be seen, however, to be statistically equivalent [8,9,14–17,46].

The basic idea is that for a given fiber we need generate only one random number once and for all, this number being its nominal lifetime t_0 under unit load as generated using Eq.

(2.8) with $L=1$. Then given its actual load history, $\ell(t) \geq L, t \geq 0$ we can determine its actual lifetime, t_ℓ, from the integral in Eq. (2.4) through solving

$$\int_0^{t_\ell} \kappa[\ell(s)]ds = t_0. \tag{2.9}$$

This is done for each fiber. Thus the main task reduces to tracking each fiber over time by way of evaluating its integral on the left-hand side of Eq. (2.9), using a continually updated version of its load history as neighbors fail and taking the upper limit as current time t. Then its own failure time is the time t_ℓ when the integral first equals t_0. This is the concept of a standard representative fiber used in previous works [14–17], and the contraction mapping in Newman *et al.* [46], which is discussed in the Appendix. Fortunately the contraction mapping can be set up so that no integration is necessary.

III. THEORETICAL RESULTS UNDER ELS

A. Mean and variance of ELS bundle lifetime

We consider the lifetime behavior of bundles under ELS because of the special role it plays in interpreting LLS for $0<\rho\leqslant 1$. Under ELS the hazard rate for the next fiber to fail after $j<N$ have already failed is

$$\lambda_j = (N-j)\kappa(K_j^{\mathrm{ELS}}L) = (N-j)\left(\frac{NL}{N-j}\right)^\rho = N^\rho (N-j)^{1-\rho} L^\rho. \tag{3.1}$$

The times ΔT_j, $j=1,\ldots,N-1$ between failures are independent and follow the exponential distribution

$$F_j(t) = 1-\exp(-\lambda_j t), \quad t \geqslant 0, \tag{3.2}$$

with respective means $\mathrm{E}[\Delta T_j]=1/\lambda_j$ and variances $\mathrm{Var}[\Delta T_j]=1/\lambda_j^2$. The bundle time to failure, T_N, is the sum of the times between failures.

The mean time to bundle failure is

$$\begin{aligned}\mathrm{E}[T_N] &= \sum_{j=0}^{N-1} \frac{1}{\lambda_j} = \frac{L^{-\rho}}{N} \sum_{j=0}^{N-1} \left(\frac{1}{1-j/N}\right)^{1-\rho} \\ &\approx L^{-\rho} \int_0^{(N-1)/N} \left(\frac{1}{1-t}\right)^{1-\rho} dt \\ &= \frac{L^{-\rho}}{\rho}\left(1-\frac{1}{N^\rho}\right).\end{aligned} \tag{3.3}$$

By similar arguments the time until a given fraction, $\phi = j/N$, of fibers has failed in a very large bundle is

$$t(\phi) = (L^{-\rho}/\rho)[1-(1-\phi)^\rho], \quad 0<\phi<1. \tag{3.4}$$

For the variance in the bundle lifetime there are various regimes for ρ. For $\rho \geqslant 1/2$ we have

$$\begin{aligned}\mathrm{Var}[T_N] &= \sum_{j=0}^{N-1} \frac{1}{\lambda_j^2} \\ &= \frac{L^{-2\rho}}{N^2} \sum_{j=0}^{N-1} \left(\frac{1}{1-j/N}\right)^{2(1-\rho)} \\ &\approx \frac{L^{-2\rho}}{N} \int_0^{(N-1)/N} \left(\frac{1}{1-t}\right)^{2(1-\rho)} dt \\ &= \frac{L^{-2\rho}}{(2\rho-1)N}\left(1-\frac{1}{N^{2\rho-1}}\right).\end{aligned} \tag{3.5}$$

For $\rho=1/2$ a similar calculation leads to

$$\mathrm{Var}[T_N] \approx \frac{L^{-1}\ln N}{N}. \tag{3.6}$$

For $0<\rho<1/2$, we obtain

$$\mathrm{Var}[T_N] \approx \frac{L^{-2\rho}}{1-2\rho}\left(\frac{1}{N^{2\rho}}-\frac{1}{N}\right). \tag{3.7}$$

Last, in the limit $\rho \to 0$ we have

$$\mathrm{Var}[T_N] \approx (1-1/N). \tag{3.8}$$

We will refer later to the standard deviation, $\mathrm{SD}[T_N]$, and the coefficient of variation, $\mathrm{CV}[T_N]$, of bundle lifetime given respectively by

$$\mathrm{SD}[T_N] = \sqrt{\mathrm{Var}[T_N]} \tag{3.9}$$

and

$$\mathrm{CV}[T_N] = \frac{\sqrt{\mathrm{Var}[T_N]}}{\mathrm{E}[T_N]}. \tag{3.10}$$

B. ELS bundle lifetime distributions

As summarized in Kelley [53], it is known for $\rho>2/3$ that the bundle lifetime T_N asymptotically follows a normal (Gaussian) distribution as $N\to\infty$ with mean $\mathrm{E}[T_N]$ and standard deviation $\sqrt{\mathrm{Var}[T_N]}$. That is, the lifetime distribution, $G_N(t)$, follows

$$G_N(t) \approx \Phi[(t-\mathrm{E}[T_N])/\sqrt{\mathrm{Var}[T_N]}], \tag{3.11}$$

where

$$\Phi(z) = \frac{1}{\sqrt{2\pi}} \int_{-\infty}^{z} e^{-y^2/2} dy. \tag{3.12}$$

This is a sufficient condition. We conjecture that this asymptotic normality holds for all $\rho \geqslant 1/2$. The difficulty in any proof, however, is that as ρ decreases the bundle lifetime becomes dominated by the last few fiber failures.

The case $\rho=1$ has special significance as a transition value in LLS. In ELS the hazard rates are $\lambda_j = NL$ for all $j=0,1,2,\ldots,N-1$. Thus the times ΔT_j between failures are independent and identically distributed following the exponential distribution with means $\mathrm{E}[\Delta T_j]=1/\lambda_j=1/(NL)$ and variances $\mathrm{Var}[\Delta T_j]=1/\lambda_j^2=1/(NL)^2$. This is true for any

load-sharing rule that conserves total bundle load (including LLS), since the sums of the hazard rates are always NL. Thus for $\rho=1$ the distribution function $G_N(t)$ is the gamma distribution

$$G_N(t)=1-e^{-NLt}\left[\sum_{j=0}^{N-1}\frac{(NLt)^j}{j!}\right], \quad t\geqslant 0, \tag{3.13}$$

with mean $\mathrm{E}[T_N]=1/L$ and variance $\mathrm{Var}[T_N]=1/(NL^2)$. Also, T_N asymptotically follows a normal (Gaussian) distribution as $N\to\infty$ with the same mean and standard deviation. That is

$$G_N(t)\approx\Phi[\sqrt{N}(Lt-1)]. \tag{3.14}$$

Because of the behavior we encounter in the next section under LLS for $\rho>1$, it is also interesting to consider

$$W_N(t)=1-[1-G_N(t)]^{1/N}, \tag{3.15}$$

for $\rho=1$ (though for ELS a slight extension applies to $\rho\geqslant 1$). According to Kelley [53] it turns out that

$$\lim_{N\to\infty} W_N(t)=\begin{cases}0, & 0\leqslant Lt<1,\\ 1-Lte^{1-Lt}, & 1\leqslant Lt.\end{cases} \tag{3.16}$$

We note that the limit is zero for $0\leqslant t<1$, which will not be true later under LLS when $\rho>1$.

For the case $\rho=0$, again ELS and LLS will yield the same results because the failure rate for fibers is independent of the loads on them.

C. Fiber failure rates under ELS for small ρ

Because of the connection between ELS and LLS for $0\leqslant\rho\leqslant 1$, we later compare their fiber failure rates in this range. Under ELS, when $j\ll N-j$, that is, $j\ll N/2$, we have

$$\begin{aligned}\lambda_j&=(N-j)\left(\frac{NL}{N-j}\right)^{\rho}\\ &=(N-j)\left(1+\frac{j}{N-j}\right)^{\rho}L^{\rho}\\ &\approx[(N-j)+j\rho]L^{\rho},\end{aligned} \tag{3.17}$$

for $j=0,1,2,\ldots$, where the last expression applies to small ρ. For $j\gg N-j$, that is, $j\gg N/2$, we have

$$\begin{aligned}\lambda_j&=(N-j)\left(\frac{NL}{N-j}\right)^{\rho}\\ &=(N-j)\left(\frac{j}{N-j}\right)^{\rho}\left(1+\frac{N-j}{j}\right)^{\rho}L^{\rho}\\ &\approx j^{\rho}(N-j)^{1-\rho}\left(1+\rho\frac{N-j}{j}\right)L^{\rho}\\ &\vdots\\ \lambda_{N-1}&=N^{\rho}L^{\rho}\approx(N-1)^{\rho}\left(1+\rho\frac{1}{N-1}\right)L^{\rho}.\end{aligned} \tag{3.18}$$

IV. THEORETICAL RESULTS UNDER LLS

A. LLS bundle lifetime behavior for $\rho>1$

In the following analysis the arguments are based on $\rho\gg 1$, though the results will work well for ρ quite close to one. Our main goal is to determine the distribution function, $G_N(t)$, for bundle lifetime where we consider the bundles to be large enough to ignore boundary effects. We begin by considering the distribution function, $G_N^{(k)}(t)$, for the time to formation of a cluster of k contiguous breaks where $k=1,2,\ldots$. Appealing to results in Tierney [15] and Phoenix and Tierney [16], we have

$$G_N^{(k)}(t)\approx 1-\exp\{-Nc_k(L)t^k\}, \tag{4.1}$$

for $t\geqslant 0$ not too large, where $c_0(L)=1$, $c_1(L)=\kappa(L)$, $c_2(L)=\kappa(L)\kappa(K_1L)$, and generally

$$c_k(L)=\frac{1}{k}\kappa(K_{k-1}L)\sum_{j=0}^{k-1}c_j(L)c_{k-j-1}(L). \tag{4.2}$$

(This result does not require $\rho\gg 1$.) Under the power-law breakdown rule we have

$$\kappa(K_jL)=K_j^{\rho}L^{\rho}, \tag{4.3}$$

so that

$$c_k(L)=L^{k\rho}c_k(1). \tag{4.4}$$

For $\rho\gg 1$, we have the approximation

$$c_k(L)\approx L^{k\rho}\frac{2^{k-1}}{k!}\prod_{j=1}^{k}K_{j-1}^{\rho}. \tag{4.5}$$

These results require time to be small enough for the k-cluster to be ''subcritical.'' Physically this means that the cluster has not yet reached the stage where it accelerates its growth and becomes a catastrophic crack, which requires additional time. A main goal is to obtain the lifetime distribution, $G_N(t)$, in the form

$$G_N(t)\approx 1-\exp\{-NW(t)\}, \quad t\geqslant 0, \tag{4.6}$$

where $W(t)$ is called the characteristic distribution function for failure of a fictitious element, which captures the local failure evolution including stress redistribution [13,14]. As a first step to estimating $W(t)$ we consider [15,16] the intersections of the k and $k+1$ versions of $G_N^{(k)}(t)$. This yields the intersection points, t_k given by

$$c_k(L)=c_{k+1}(L)t_k, \quad k\geqslant 1, \tag{4.7}$$

which reduces for $\rho\gg 1$ to

$$t_k\approx L^{-\rho}\left(\frac{k+1}{2}\right)\left(\frac{2}{k+2}\right)^{\rho}. \tag{4.8}$$

We then consider the sequence of values W_k^* defined as

$$W_k^* = c_k(L) t_k^k$$
$$= L^{k\rho} \frac{1}{k!} 2^{k-1} \prod_{j=1}^{k} \left(\frac{j+1}{2}\right)^{\rho} L^{-k\rho} \left(\frac{k+1}{2}\right)^{k} \left(\frac{2}{k+2}\right)^{k\rho}$$
$$= \left[\frac{(k+2)!}{(k+2)^{k+2}}\right]^{\rho-1} (k+2)^{\rho-1} \left(\frac{k+1}{k+2}\right)^{k+1} \frac{k+2}{2}, \quad (4.9)$$

where $k=1,2,\ldots$. By Stirling's formula,

$$(k+2)! \sim \sqrt{2\pi}(k+2)^{k+2+1/2} e^{-(k+2)}, \quad (4.10)$$

and thus

$$W_k^* \approx \frac{(\sqrt{2\pi})^{\rho-1}}{2} (k+2)^{(\rho-1)/2} e^{-(k+2)(\rho-1)}$$
$$\times (k+2)^{\rho} e^{-(k+1)/(k+2)}$$
$$\approx \frac{(\sqrt{2\pi})^{\rho-1}}{2} (k+2)^{(3\rho-1)/2} e^{-(k+2)(\rho-1)-1}. \quad (4.11)$$

Next we obtain a relationship between k and t_k, and we see from Eq. (4.8) that

$$k = k(t) \approx 2(L^{\rho} t)^{-1/(\rho-1)} - 2, \quad (4.12)$$

where we have dropped the subscript k on t. Letting $W^*(t) = W^*_{k(t)}$ we thus obtain

$$W^*(t) \approx C^* \left(\frac{a}{L^{\rho} t}\right)^{\phi^*/(\rho-1)} \exp\left[-(\rho-1)\left(\frac{a}{L^{\rho} t}\right)^{1/(\rho-1)}\right], \quad (4.13)$$

where

$$\phi^* = \frac{3\rho-1}{2}, \quad (4.14)$$

$$a = 2^{\rho-1}, \quad (4.15)$$

and

$$C^* = \frac{(\sqrt{2\pi})^{\rho-1}}{2e}. \quad (4.16)$$

This is our first approximation to $W(t)$, which is based on the time to formation of a critical k-cluster at time t as though the bundle then fails instantaneously [15,16].

We can also speak of a critical cluster size, k^*, which is the value of $k(t)$ that solves $NW^*_{k(t)} = 1$. Roughly speaking k^* is the cluster size at the onset of failure of a ''typical'' specimen (with lifetime close to the median lifetime) of size N. It can be shown by inverting this expression that k^* depends on N following

$$k^* + 2 = \frac{\ln(C^* N)}{\rho-1}(1+\varepsilon_N^*), \quad (4.17)$$

where

$$\varepsilon_N^* \approx \frac{\phi^*\{\ln[\ln(C^*N)] - \ln(2\rho-2)\}}{\ln(C^*N) - \phi^*}. \quad (4.18)$$

So far we have considered the distribution for the time to critical cluster formation. However, as noted by Curtin and Scher [41], it takes significant additional time for the cluster to become catastrophic. To gain insight into this time difference we adapt to the present setting a solution by Yaschin [54] and Feigin and Yaschin [55] for power-law growth of a one-direction sequence of failures of fresh elements. Making this correspondence requires $\rho \gg 1$. First we write out their solution using their hazard rates written in a form that can be matched to ours for a growing failure cluster in a bundle, which can grow in either direction. We then write out all the idealized local load-sharing versions of the hazard rates, and then match these to those used in the Feigin–Yaschin (FY) solution. Finally we make adjustments for those entries where matching does not occur.

To adapt the FY result, we take (in our notation and correcting a minor algebraic error)

$$\lambda_j^{\mathrm{FY}} = L^{\rho} 2^{1-\rho} (j+1)^{\rho}, \quad j = 0,1,2,\ldots, \quad (4.19)$$

and write their result as

$$W^{\mathrm{FY}}(t) \approx \frac{2}{(\sqrt{2\pi})^{1-\rho}} \sqrt{\frac{\rho}{\rho-1}} \left(\frac{a}{tL^{\rho}}\right)^{1/2}$$
$$\times \exp\left\{-\gamma(\rho)(\rho-1)\left(\frac{a}{tL^{\rho}}\right)^{1/(\rho-1)}\right\}, \quad (4.20)$$

where

$$\gamma(\rho) = \left[\frac{\sin(\pi/\rho)}{\pi/\rho}\right]^{\rho/(1-\rho)}. \quad (4.21)$$

In the case of LLS, the hazard rates are given by

$$\lambda_0 = L^{\rho} = \frac{1}{2} L^{\rho} 2^{1-\rho} (2)^{\rho}, \quad (4.22)$$

and

$$\lambda_j = L^{\rho} 2^{1-\rho} (j+2)^{\rho}, \quad j = 1,2,3,\ldots, \quad (4.23)$$

since for a contiguous cluster of j breaks $K_j = (j+2)/2$ and there are two overloaded flanking fibers at risk. These can be connected to those of FY by noting that

$$\lambda_0 = \frac{1}{2} \lambda_1^{\mathrm{FY}} \quad (4.24)$$

and

$$\lambda_j = \lambda_{j+1}^{\mathrm{FY}}, \quad j = 1,2,3,\ldots . \tag{4.25}$$

The main difference between the FY case and LLS is that in LLS there is no equivalent element with failure with rate λ_0^{FY}, and the failure rate in LLS corresponding to λ_1^{FY} is actually half that value. This occurs because, when $\rho \gg 1$, a failure sequence in LLS involves one initiator followed by propagation through neighbors of which there are always two choices, one on each side. The latter difficulty can be treated by thinking in terms of $N/2$ fibers rather than N fibers, and the former by dividing their result by $2^{1-\rho} t L^{\rho}$. This is seen by studying the appropriate convolution and recognizing that, in the FY case, the total time can be decomposed into an initiation time under hazard rate λ_0^{FY} and a propagation time involving the sums of the times under the remaining hazard rates $\lambda_1^{\mathrm{FY}}, \lambda_2^{\mathrm{FY}}, \ldots$.

With these constructions, we estimate $W(t)$ as

$$\hat{W}(t) \approx \hat{C}\left(\frac{a}{tL^{\rho}}\right)^{\hat{\phi}/(\rho-1)} \exp\left\{-\gamma(\rho)(\rho-1)\left(\frac{a}{tL^{\rho}}\right)^{1/(\rho-1)}\right\}, \tag{4.26}$$

where

$$\hat{C} = (\sqrt{2\pi})^{\rho-1}\sqrt{\frac{\rho}{\rho-1}} \tag{4.27}$$

and

$$\hat{\phi} = 3(\rho-1)/2, \tag{4.28}$$

and again $a = 2^{\rho-1}$.

This result differs from the result for $W^*(t)$ obtained earlier for the time to form a critical cluster k^*. The key difference is the introduction of the factor $\gamma(\rho)$ in the exponential. There is also a lesser difference between $\hat{\phi}$ and ϕ^* and a small difference between $\hat{C}$ and C^*. The main effect is captured, however, in noting that

$$\gamma(\rho)\left(\frac{a}{L^{\rho}t}\right)^{1/(\rho-1)} = \left[\frac{a}{\gamma(\rho)^{-(\rho-1)}L^{\rho}t}\right]^{1/(\rho-1)} \tag{4.29}$$

and

$$\gamma(\rho)^{-(\rho-1)} = \left[\frac{\sin(\pi/\rho)}{\pi/\rho}\right]^{\rho} \approx 1 - \pi^2/(6\rho). \tag{4.30}$$

The existence of the factor $\gamma(\rho)$ compared with unity has the effect of lengthening the characteristic time to failure $\hat{t}_f$ as compared to the characteristic time t^* to critical cluster formation, obtained by solving $N\hat{W}(\hat{t}_f) = 1$ and $NW^*(t^*) = 1$, respectively. The result is

$$\hat{t}_f \approx \frac{t^*}{\{[\sin(\pi/\rho)]/(\pi/\rho)\}^{\rho}} \approx \frac{t^*}{1-\pi^2/(6\rho)}. \tag{4.31}$$

Note from the middle expression that the two times diverge as $\rho \to 1$ from above.

We can also determine the size effect for the characteristic failure time, $\hat{t}_f$. Upon inverting $N\hat{W}(t_f) = 1$ asymptotically, we obtain

$$\hat{t}_f \approx aL^{-\rho}\left[\frac{\rho-1}{\ln(\hat{C}N)(1+\hat{\varepsilon}_N)}\right]^{\rho-1}, \tag{4.32}$$

where

$$\hat{\varepsilon}_N \approx \frac{\hat{\phi}\{\ln[\ln(\hat{C}N)] - \ln(\rho-1)\}}{\ln(\hat{C}N) - \hat{\phi}}. \tag{4.33}$$

Here $\hat{t}_f$ is also approximately the median lifetime. Even with the correction $\hat{\varepsilon}_N$, accuracy of this result requires N large whereby $\ln(\hat{C}N) \gg \hat{\phi} = 3(\rho-1)/2$. This points to the difficulty in using Monte Carlo simulations on bundles of limited size to reveal true large-scale behavior.

B. LLS bundle lifetime behavior for $0 < \rho \leqslant 1$

We begin by considering the case $\rho = 1$, wherein the fiber failure rate is exactly the load on it. Since the fibers are statistically independent and their loads sum to the bundle load NL, the failure rate for the jth fiber to fail, irrespective of position and given that $j-1$ have already failed, is also NL. Thus this failure rate is independent of the number and configuration of failed fibers up to that point. Thus LLS has the same distribution for times between successive fiber failures as ELS, as mentioned earlier. Thus the lifetime distribution for the bundle, $G_N(t)$, is also given by Eq. (3.13) and asymptotically by Eq. (3.14). (This is not true, however, when $\beta \neq 1$.) This result for $\rho = 1$ suggests that ELS will play a key role in the regime $0 < \rho \leqslant 1$.

Despite this equivalence in bundle lifetime for $\rho = 1$, a difference between LLS and ELS is that fiber failures will be more clustered in LLS where there will be more large clusters and fewer small clusters. The failure rates for fibers next to clusters are always higher than for survivors with no failed neighbors. Under ELS clustering will be totally at random with a pattern as in 1D percolation with $N-j$ broken fibers. Also in LLS the spectrum of loads carried by surviving fibers for $j = 1, \ldots, N-1$ will be spread out whereas in ELS, all the loads are simply $NL/(N-j)$. Extending our earlier result, Eq. (4.2), under LLS for $\rho > 1$ to the present case of $\rho = 1$, we see that the number of clusters of size k at time t is approximately $Nc_k(1)(Lt)^k$ where $c_0(1) = 1$ and

$$c_k(1) = \frac{k+1}{2k}\sum_{j=0}^{k-1} c_j(1)c_{k-j-1}(1). \tag{4.34}$$

From this we could estimate the LLS load spectrum.

For $0 < \rho < 1$ we have no theory for the lifetime distribution under LLS except to say that we will find computationally, and supported by fiber failure rate arguments presented next, that the differences between ELS and LLS will be minor.

C. Fiber failure rates under LLS for small ρ

The fiber failure rate for $0 \leqslant j \ll N$ is

$$\lambda_0 L^{-\rho} = N, \tag{4.35}$$

$$\begin{aligned}\lambda_1 L^{-\rho} &= (N-3) + 2\left(1+\frac{1}{2}\right)^{\rho} \\ &= N-1+2\left\{\left(1+\frac{1}{2}\right)^{\rho}-1\right\} \\ &\approx N-1+\rho\, 2\ln(3/2)+\mathcal{O}(\rho^2),\end{aligned} \tag{4.36}$$

$$\begin{aligned}\lambda_2 L^{-\rho} &= (N-6) + 4\left(1+\frac{1}{2}\right)^{\rho} \\ &= N-2+4\left\{\left(1+\frac{1}{2}\right)^{\rho}-1\right\} \\ &\approx N-2+2\rho\, 2\ln(3/2)+\mathcal{O}(\rho^2), \\ &\vdots\end{aligned} \tag{4.37}$$

$$\lambda_j L^{-\rho} \approx N-j+j\rho\, 2\ln(3/2)+\mathcal{O}(\rho^2), \tag{4.38}$$

where the latter approximations in each case require $0<\rho \ll 1$. These approximations require the breaks to be well separated, which implies that failures of fresh fibers are much more likely than failures in fibers next to old breaks, which basically means that $N-j \gg j\rho\, 2\ln(3/2)$. Under ELS, we recall from Eq. (3.17) that $\lambda_j L^{-\rho} \approx N-j+j\rho$. Also as $\rho \to 1$, it can be shown that $\lambda_j L^{-\rho} \approx N+j3(\rho-1)\ln(3/2)$ as compared to $\lambda_j L^{-\rho} \approx N+j(\rho-1)$ for ELS. Thus for $0<\rho \ll 1$ the hazard rates are only slightly smaller under LLS than under ELS.

Next we look at $1 \ll j \leqslant N$, and we note first that for any configuration of ''X''s and ''O''s, i.e., failed and surviving fibers, if there are strings of ''X''s then the hazard rate is less than if all ''X''s are isolated, because

$$(2k-2)+2\left(1+\frac{k}{\rho}\right)^{\rho} < 2k\left(1+\frac{1}{\rho}\right)^{\rho}. \tag{4.39}$$

But as j increases there will be many strings of ''X''s and eventually as $j \to N$, only isolated ''O''s exist. In that case we consider strings like

$$\cdots \mathrm{O} \underbrace{\mathrm{XX}\cdots\mathrm{X}}_{k-i} \mathrm{O} \underbrace{\mathrm{XXX}}_{i} \mathrm{O}\cdots \tag{4.40}$$

and let

$$p = j/N, \quad q = 1-j/N. \tag{4.41}$$

Then given surviving fiber ''O'' sandwiched between strings of breaks ''X''s as above, the probability it has exactly k broken neighbors is $(k+1)q^2p^k$.

This result assumes breaks are positioned at random, which is approximately true for small ρ. (For ρ nearer to 1 there could be a small difference because ''X''s will tend to clump more as they develop.) We have

$$\begin{aligned}\lambda_j L^{-\rho} &\approx Nq\sum_{k=0}^{\infty}(k+1)\left(\frac{k+2}{2}\right)q^2p^k \\ &= \frac{Nq^3}{2^{\rho}p^2}\left\{\sum_{k=0}^{\infty}(k+2)^{\rho+1}p^{k+2}-\sum_{k=0}^{\infty}(k+2)^{\rho}p^{k+2}\right\} \\ &= \frac{Nq^3}{2^{\rho}p^2}\left\{\sum_{k=0}^{\infty}k^{\rho+1}p^{k}-\sum_{k=0}^{\infty}(k+2)^{\rho}p^{k}\right\}.\end{aligned} \tag{4.42}$$

Moreover,

$$\begin{aligned}\sum_{k=0}^{\infty}k^{\alpha}p^k &\approx \int_0^{\infty}t^{\alpha}\exp[-t\ln(1/p)]dt \\ &= \{\ln[1/(1-q)]\}^{\alpha+1}\Gamma(\alpha+1) \\ &\approx (1/q)^{\alpha+1}\alpha\Gamma(\alpha),\end{aligned} \tag{4.43}$$

so under LLS,

$$\begin{aligned}\lambda_j L^{-\rho} &\approx \frac{Nq^3}{2^{\rho}p^2}\left\{\frac{1}{q^{\rho+2}}(\rho+1)\Gamma(\rho+1)-\frac{1}{q^{\rho+1}}\rho\Gamma(\rho)\right\} \\ &= Nq^{1-\rho}\left[\frac{1}{2^{\rho}(1-q)^2}\right]\Gamma(\rho+1)[(\rho+1)-q].\end{aligned} \tag{4.44}$$

When $0<\rho \ll 1$, however, we have

$$\frac{1}{2^{\rho}(1-q)^2}\Gamma(\rho+1)\{(\rho+1)-q\} \approx \frac{2^{-\rho}}{p}, \tag{4.45}$$

since $p=1-q$, so we see that

$$\lambda_j L^{-\rho} \approx Nq^{1-\rho}\frac{1}{2^{\rho}p}, \tag{4.46}$$

compared to the ELS result, Eq. (3.18), rewritten as

$$\lambda_j L^{-\rho} = Nq^{1-\rho}. \tag{4.47}$$

So there is little difference between ELS and LLS as $j \to N$ since $p = j/N \to 1$.

Note that for $\rho = 1$, the LLS result is

$$\lambda_j L^{-\rho} = \frac{Nq^3}{2}\sum_{k=0}^{\infty}(k+1)(k+2)p^k = \frac{Nq^3}{2}\frac{2}{(1-p)^3} = N, \tag{4.48}$$

as it should be.

In summary, in comparing times ΔT_j between fiber failures in LLS and ELS, there is no difference in fiber failure rates for $\rho=0$ and $\rho=1$, and for $0<\rho<1$ there is little difference at the extremes $0 \leqslant j \ll N$ and $j \to N$. Actually $j \to N$ is most important because the ΔT_j's are relatively the longest there. Thus LLS may give slightly longer bundle failure times T_N than ELS, but the shapes of the distributions should be similar.

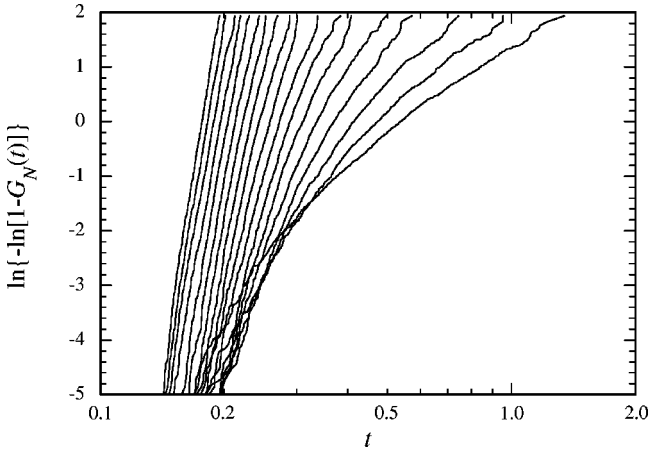

FIG. 1. Cumulative distribution function, $G_N(t)$, for LLS bundle failure time for fiber exponent $\rho=2$, and bundle sizes $N=8,16,32,64,\ldots,1\,048\,576$ (1024 replications each). Times shown in all figures are dimensionless.

D. Lifetime behavior for $0 \ll \rho \ll 1$

When $\rho=0$, the fiber failure rates are all the same since $\kappa(K_rL)=(K_rL)^0=1$, and the times between fiber failures have rates

$$\lambda_j = N-j, \quad j=0,1,\ldots,N-1. \tag{4.49}$$

By definition, the lifetime of the bundle is just the maximum lifetime found among the fibers, so that

$$G_N(t)=(1-e^{-t})^N \approx \exp(-Ne^{-t})=\exp[-e^{-(t-\ln N)}]. \tag{4.50}$$

The median lifetime $\hat{t}_{N,1/2}$, from $G_N(\hat{t}_{N,1/2})=1/2$, is

$$\hat{t}_{N,1/2} \sim \ln N - \ln\ln 2. \tag{4.51}$$

The α-spread of the distribution defined as $\Delta\hat{t}_{N,\alpha}=\hat{t}_{N,(1-\alpha)}-\hat{t}_{N,\alpha}$ where $0<\alpha<1/2$ and generally $G_N(\hat{t}_{N,p})=p, 0<p<1$, can be seen to satisfy

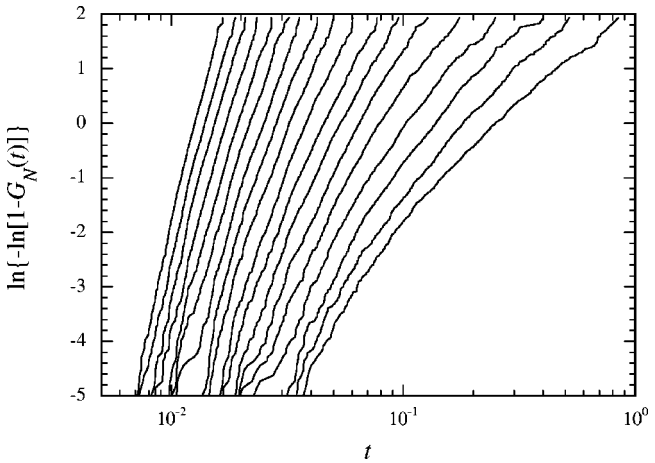

FIG. 2. $G_N(t)$ under the same conditions as in Fig. 1 except $\rho=4$.

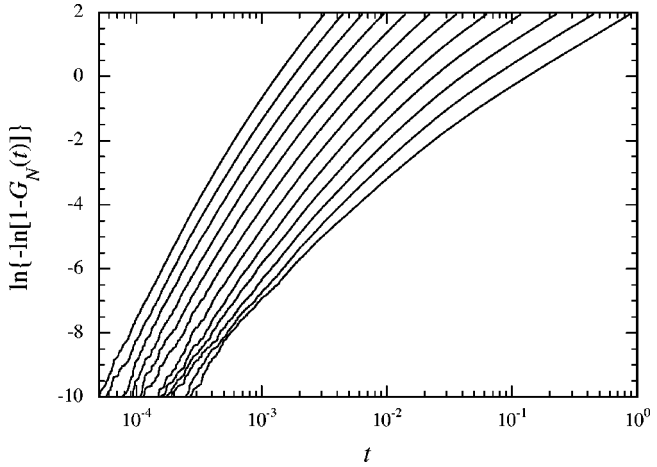

FIG. 3. $G_N(t)$ under the same conditions as in Fig. 1 except $\rho=10$, the largest N is 16 384 and the replications are 262 144.

$$\Delta\hat{t}_{N,\alpha} \sim \ln\left[\frac{\ln(\alpha)}{\ln(1-\alpha)}\right], \tag{4.52}$$

and so is independent of N. Earlier, we argued in Eq. (3.8) that $\mathrm{Var}[T_N]=1-1/N$.

For very small ρ we conjecture that the lifetime distribution of the bundle will approximately follow

$$G_N(t) \approx \exp\left\{-\exp\left[-\left(\frac{t-\mathrm{E}[T_N]}{\sqrt{\mathrm{Var}[T_N]}}\right)\right]\right\}. \tag{4.53}$$

The idea is that the lifetime is dominated by some long-lived cluster of fibers, which grows slowly in size as N increases but not enough to compensate for the extra load it eventually must support as fibers fail. This will be investigated using computational simulations.

We turn our attention to a detailed comparison between the statistical failure theories for LLS and ELS and exact Monte Carlo simulations. Computational methods needed to obtain these results in hours-to-days, rather than decades-to-centuries, are provided in the Appendix.

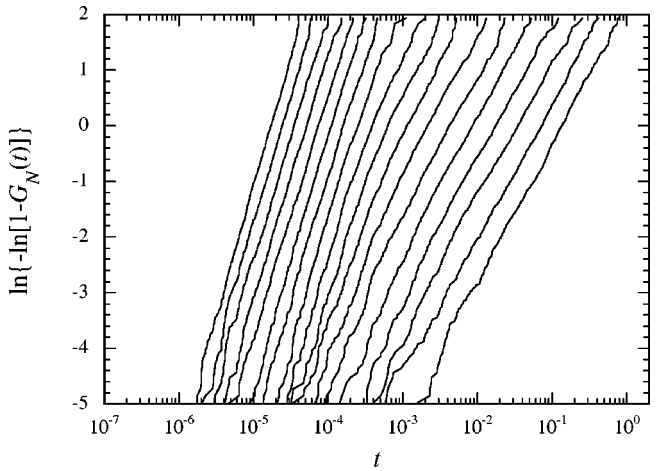

FIG. 4. $G_N(t)$ under the same conditions as in Fig. 1 except $\rho=20$.

V. COMPUTATIONAL RESULTS

In all the results that follow, we have taken the load L to be unity, with no loss in generality, since t can be replaced by tL^{ρ} to recover results for arbitrary L.

A. Bundle lifetime behavior for $\rho>1$

Figures 1–4 show empirical plots of the cumulative distribution function (c.d.f.) for bundle lifetime, $G_N(t)$, versus t for the cases $\rho=2$, 4, 10, and 20. The coordinates are Weibull coordinates wherein $\ln\{-\ln[1-G_N(t)]\}$ is plotted versus $\ln(t)$ on a linear scale [though for convenience a $\log_{10}(t)$ scale has been used]. Each figure has bundles sizes $N=8,16,32,64,\ldots,1\,048\,576$ with 1 024 Monte Carlo replications each, except for Fig. 3 which has maximum $N=16\,384=2^{14}$ but with $262\,144=2^{18}$ replications each (though due to the huge size of the data set, in each curve the first 1024 points were plotted but only one out of every 256 points thereafter). For convenience, we will refer to $1\,048\,576=2^{20}$ fibers in a bundle as a million fiber bundle, and $1\,024=2^{10}$ as a thousand realizations. In all cases the deep tails have been truncated so as not to show the bottom seven points (12 in Fig. 3) in order to subdue their typical erratic behavior.

Clearly all cases of ρ show a size effect as the probability of failure increases with N. If $G_N(t)$ were truly a Weibull distribution, $1-\exp[-(t/t_{0,N})^{\alpha_N}]$ with shape parameter, α_N, and scale parameter, $t_{0,N}$, the plots would be straight lines with slope α_N and value 0 at $\ln(t_{0,N})$. The lack of linearity in all cases (except perhaps for the smallest and largest bundles for $\rho=20$) indicates that $G_N(t)$ is not Weibull. Note, however, that locally the slopes of these curves are generally multiples of one, the Weibull shape parameter for a single fiber element under fixed load, according to Eq. (2.8). The exception is the upper part of the lifetime distributions for very small bundles in the case of $\rho=10$, and 20, where the slope is clearly unity even near the median lifetime (corresponding to -0.367 on the vertical scale). This suggests that, except perhaps for the shortest-lived bundles, once one fiber fails the whole bundle quickly fails so that the bundle acts like a chain of N fibers whereby the median would be roughly $1/N$, as is observed in the plots.

In the deep tails of the distributions, convergence and even crossovers for the smallest bundles may occur if the number of replications is sufficiently large (i.e., low enough probability level) because of boundary and finite size effects. For very small N, bundle failures in the deep tails are likely to begin with fibers failing at or near the bundle edges. These then generate clusters that rapidly propagate across the bundle since the load is shed totally to the nearest interior survivor rather than being divided equally between two flanking survivors.

The lower tail crossing effect is very apparent in Fig. 1 for $\rho=2$. A Weibull tangent to the lower tail of the $N=32$ fiber bundle (at probability level 1/150) has a Weibull shape parameter of approximately 10, whereas that for the $N=8$ bundle is approximately the same number, 8. The latter correspondence is to be expected once the critical cluster size for a bundle reaches its width. This limiting aspect of the slope is the cause of the crossing. For the largest bundle with $\rho=2$, the Weibull tangent has a much larger exponent of about 25 in the deep tail, so a cluster of approximately 25 breaks is required to nucleate a catastrophic crack. While there is noticeable convergence in Figs. 2–4, the potential lower tail crossing effect is not apparent because the curves do not go deep enough into the lower tails, even in Fig. 3. For example in Fig. 2 where $\rho=4$, the curve for the million fiber bundle is roughly Weibull with shape parameter (slope) 4. Thus the lifetime is approximately determined when a critical cluster of four adjacent breaks is formed, and true crossovers will not occur since such a cluster is well contained within the smallest bundles. In Fig. 3 for $\rho=10$, which goes much deeper into the lower tails, convergence is again apparent, but again not true crossing. Weibull tangents to the deep tails for $N=8$ and 16 have exponents of approximately 3, which again is considerably less than the bundle

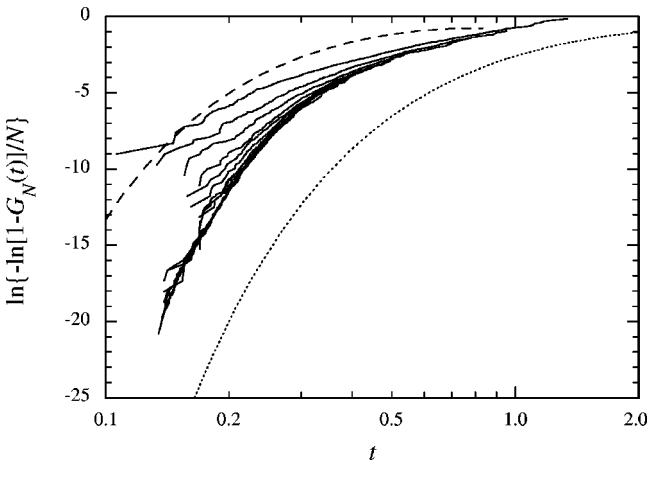

FIG. 5. Cumulative distribution functions $W_N(t)$ (solid lines) on Weibull coordinates, which are reverse weakest link transforms of $G_N(t)$ in Fig. 1 for $\rho=2$. The dotted line is the approximation $\hat{W}(t)$, and the dashed line is the approximation $W^*(t)$ to the true characteristic distribution function $W(t)$.

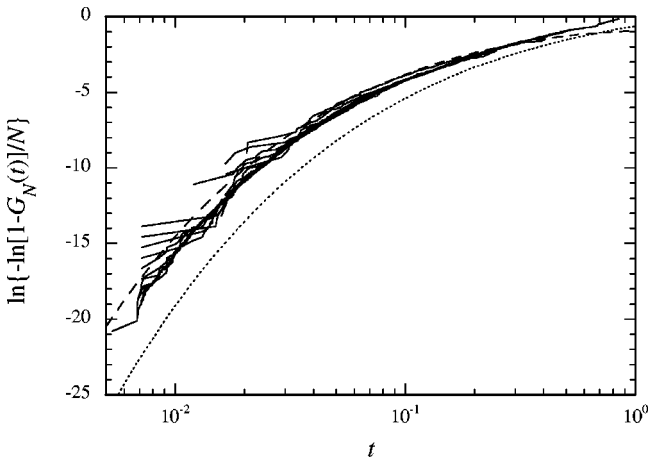

FIG. 6. $W_N(t)$ (solid lines), $\hat{W}(t)$ (dotted line), and $W^*(t)$ (dashed line) under the same conditions as in Fig. 5 except $\rho=4$ and $G_N(t)$ comes from Fig. 2.

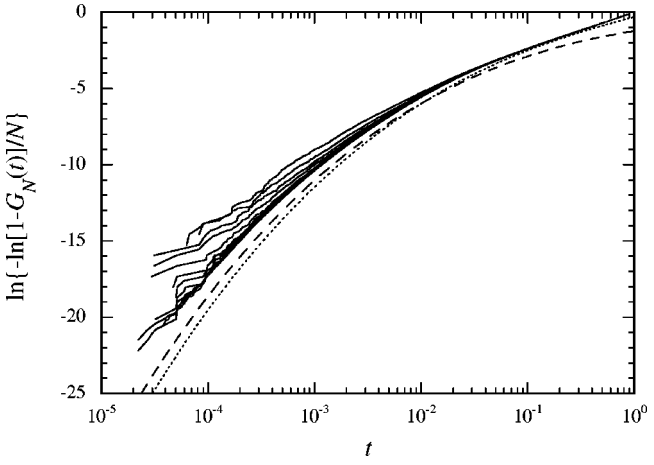

FIG. 7. $W_N(t)$ (solid lines), $\hat{W}(t)$ (dotted line), and $W^*(t)$ (dashed line) under the same conditions as in Fig. 5 except $\rho=10$ and $G_N(t)$ comes from Fig. 3.

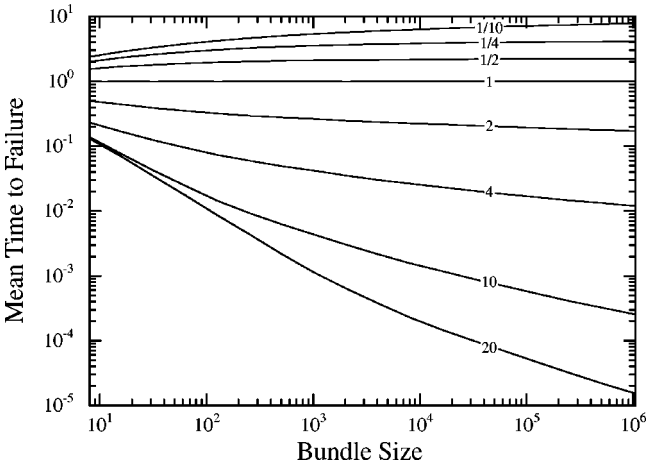

FIG. 9. Mean time to bundle failure, $E[T_N]$, versus LLS bundle size N with 1024 replications for $\rho=1/10$, 1/4, 1/2, 1, 2, 4, 10, and 20.

widths. In Fig. 4 with $\rho=20$, when N is very small the Weibull tangent has slope near unity. Thus in this probability range, once one fiber fails the whole bundle fails. When N is large (say one million fibers), the Weibull exponent is 2, so two adjacent failures fail the bundle. In these cases the empirical plots are approximately Weibull except for the middle sizes where there is bilinear behavior, discussed later.

Figures 5–8 show plots of the reverse weakest link transform, $W_N(t)=1-[1-G_N(t)]^{1/N}$, of the data in Figs. 1–4, on Weibull coordinates. The idea is that if $W_N(t)$ converges to a limit $W(t)$ as N grows large, then $G_N(t)\approx 1-[1-W(t)]^N$. On Weibull coordinates, the differences between the $G_N(t)$ for each N would appear as vertical shifts of magnitude $\ln N$, which is what is seen in Figs. 1–4. Except for small bundle and boundary effects, these clearly disappear in Figs. 5–8. Also shown are the two approximations to the characteristic distribution function, $\hat{W}(t)$ and $W^*(t)$, given by Eqs. (4.26) and (4.13), respectively, where the latter is based on time to critical cluster formation. For $\rho>4$ these two versions of the true $W(t)$ perform very well with the one based on time to critical cluster formation being more conservative. For higher ρ values, neither approximation is sufficiently conservative, i.e., both overestimate the time to achieve a given probability of failure by roughly a constant factor somewhat greater than one. This occurs because many possible failure sequences, such as linking of smaller clusters, are not accounted for. For $\rho=2$, one is too conservative and the other not conservative enough, but the error is less than might first appear as the time scale is greatly expanded.

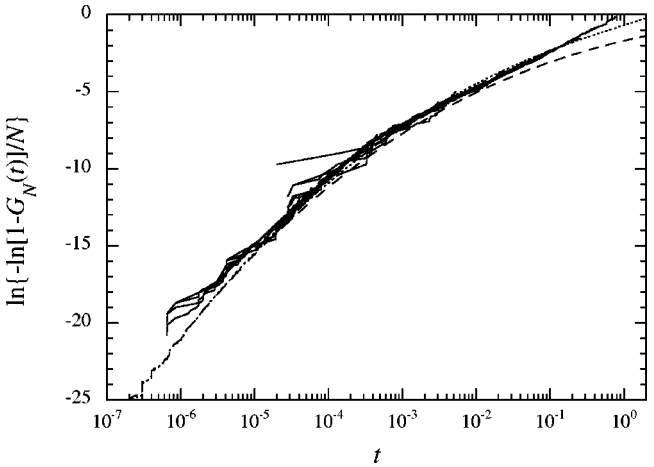

FIG. 8. $W_N(t)$ (solid lines), $\hat{W}(t)$ (dotted line), and $W^*(t)$ (dashed line) under the same conditions as in Fig. 5 except $\rho=20$, where $G_N(t)$ comes from Fig. 4.

In Figs. 5–8 the time difference between the two versions $\hat{W}(t)$ and $W^*(t)$ is essentially the additional time required for catastrophic growth of the critical cluster. For larger ρ the time difference is slight compared to the time to form the critical cluster, but for $\rho=2$ the time difference is by a factor of about 2.5, as can be seen also from Eq. (4.31). This factor rapidly grows to ∞ as $\rho\to 1$ from above. For $\rho=10$ the difference is only about 20% in the deep tail [slightly less than the difference between $W^*(t)$ and the empirical $W(t)$]. Thus for $\rho>4$, these estimates give good agreement with the true $W(t)$, which is quite reasonable even for $\rho=2$. In Fig. 8 there is clearly bilinear behavior in the empirical plots for $\rho=20$, and the Weibull segments have slopes exactly one and two, respectively, consistent with the corresponding critical cluster sizes of one and two.

A key conclusion from Figs. 1–8 is that for $\rho>1$, the lifetime distribution has the basic weakest-link structure $G_N(t)=1-[1-W(t)]^N\approx 1-\exp[-NW(t)]$. Thus LLS behavior differs from that under ELS, where the lifetime is asymptotically Gaussian, Eq. (3.11), with mean, Eq. (3.3), which converges to a finite limit $1/\rho$ as $N\to\infty$.

Figures 9–11 show plots of the empirical mean, standard deviation, and coefficient of variation of lifetime (standard deviation/mean), as a function of N on log-log coordinates for $\rho=2$, 4, 10, and 20. The plots are based on 1024 replications each for $N=8,16,32,64,\ldots,1\,048\,576$. The mean does not follow the ELS mean, Eq. (3.3), where the lifetime approaches $1/\rho$ for large N, though for $\rho=2$, the difference is minor for small N. The mean also does not follow a power

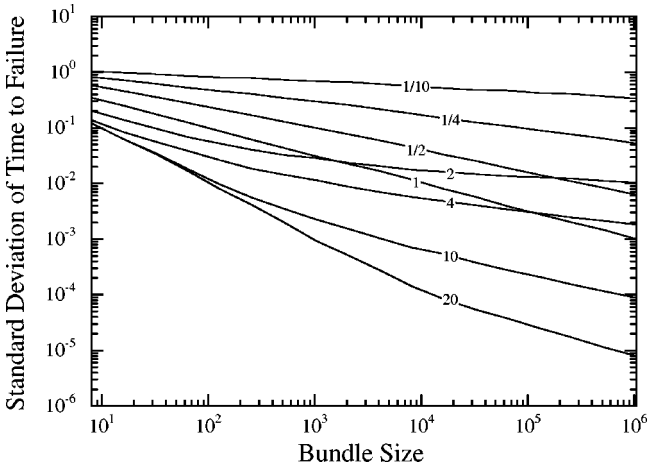

FIG. 10. Standard deviation of time to bundle failure, SD$[T_N]$, versus LLS bundle size N under the same conditions as in Fig. 9.

law in N, but ultimately scales as $a[(\rho-1)/\ln N]^{(\rho-1)}$, according to Eq. (4.32), though the error term is important even for the largest values of N. The standard deviation ultimately scales as $a[(\rho-1)/\ln N]^{\rho}$, and the coefficient of variation, being approximately the inverse of the critical cluster size k^*, ultimately scales as $(\rho-1)/\ln N$ according to Eq. (4.17). For $\rho=20$, the rapid drop in the coefficient of variation at about $N=3000$ is not an artifact. In fact the coefficient of variation is approximately 1 for $1\leqslant N\leqslant 2000$ corresponding to $k^*=1$, and becomes 1/2 over roughly $5\,000\leqslant N \leqslant 1\,000\,000$, corresponding to $k^*=2$. This feature is consistent with the kink observed in Fig. 8. In essence, these values of N are too small for the large scale trend to take over. The LLS standard deviation also behaves very differently from the corresponding ELS one that decays as $1/\sqrt{N}$, Eq. (3.5).

Figure 12 shows plots of empirical fiber failure times versus fraction of failed fibers in a single LLS bundle with 4096 fibers (solid lines) and $\rho=2$. Also shown is this fraction as calculated from ELS theory, Eq. (3.4) (dotted lines). Note that LLS behavior diverges from ELS behavior as LLS

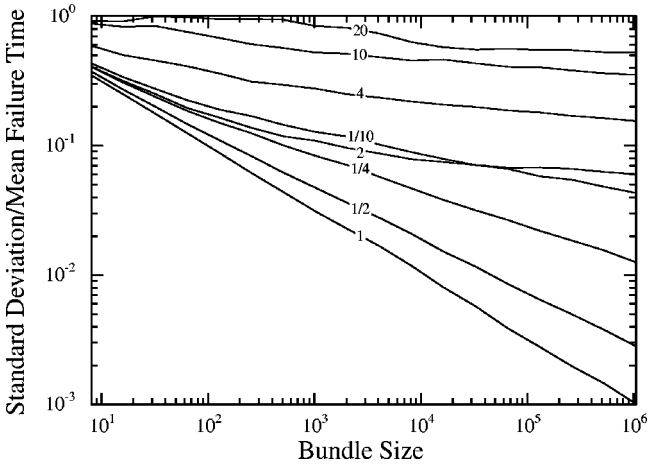

FIG. 11. Coefficient of variation of time to bundle failure, CV$[T_N]$, versus LLS bundle size N under the same conditions as in Fig. 9.

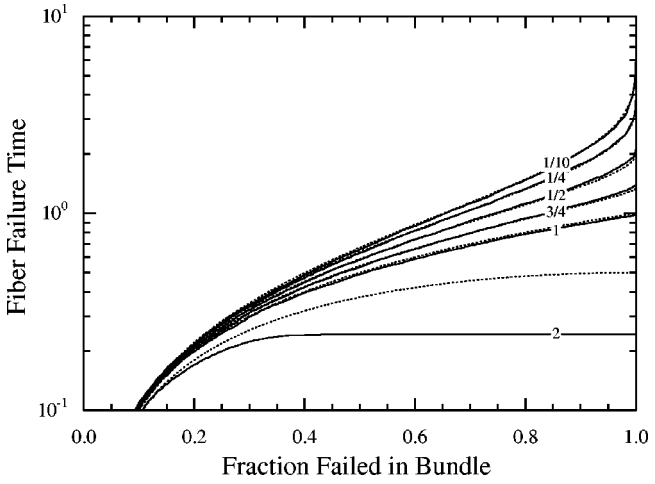

FIG. 12. Empirical fiber failure times versus fraction of failed fibers in a single bundle with $N=4096$ fibers. Solid lines are for LLS bundles and dotted lines are for ELS bundles.

shows the rapid collapse due to increasing local stress concentrations around a cluster that becomes catastrophic once about 1/4 of the fibers fail. If the bundle size were increased by orders of magnitude, the $\rho=2$ curve would be the same at a very small fraction of failures but would flatten before the fraction 1/4 as the bundle failed earlier due to the size effect. These effects would be even more pronounced for larger ρ and the critical fraction would decrease sharply.

B. Bundle lifetime behavior for $1/2\leqslant\rho<1$

Figures 13 and 14 show empirical plots of the c.d.f. for bundle lifetime, $G_N(t)$, versus normalized time t_{norm}, for the cases $\rho=0.5$ and 0.75, respectively. We employ ''Gaussian coordinates,'' i.e., the ordinate is scaled so that a normal or Gaussian distribution will appear to be a straight line. Moreover, we normalized the lifetime data, by subtracting the sample mean and dividing by the sample standard deviation,

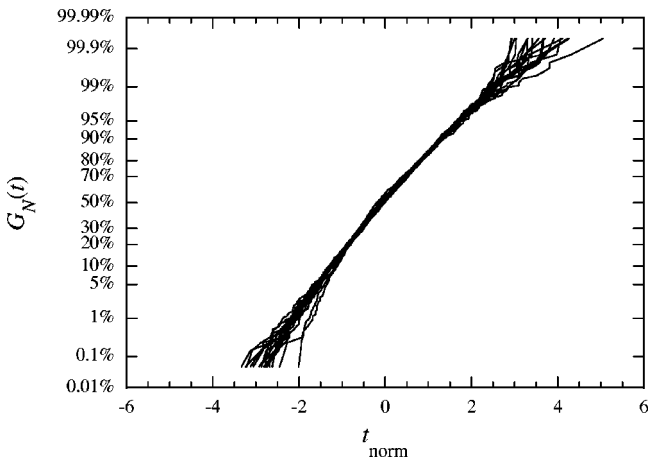

FIG. 13. Cumulative distribution function $G_N(t)$ for LLS bundle failure time plotted on Gaussian coordinates versus normalized bundle failure time, t_{norm} (actual time minus sample mean then divided by sample standard deviation) for $\rho=0.5$ and bundle sizes $N=8,16,32,64,\ldots,1\,048\,576$ (1024 replications each).

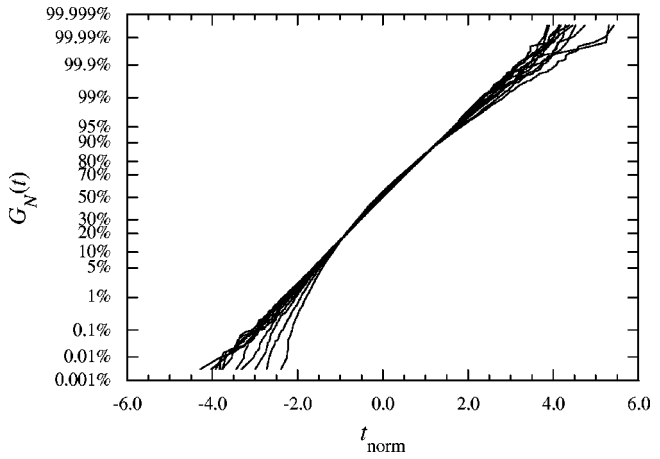

FIG. 14. $G_N(t)$ under the same conditions as in Fig. 13 except $\rho=0.75$, the largest bundle has 16 384 fibers and the number of replications is 16 384.

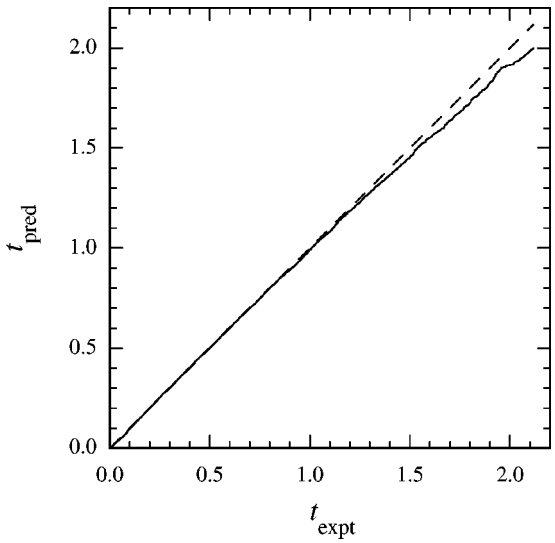

FIG. 15. Predicted fiber failure times, t_{pred}, in a large ELS bundle versus empirical fiber failure times, t_{expt}, observed in an LLS bundle with 4096 fibers and $\rho=0.5$. Times were evaluated at equivalent fractions of failed fibers in the bundle.

for each N. The scaled t_{norm}, therefore, has zero mean and unit variance. For $\rho=0.75$, the bundles sizes were $N=8,16,32,64,\ldots,16\,384$ with 16 384 replications each, and for $\rho=1/2$ the bundle sizes were $8,16,32,\ldots,1\,048\,576$, but with 1024 replications each. If the distributions, $G_N(t)$, were truly normal, on these Gaussian coordinates they would overlay each other onto one straight line corresponding to zero mean and unit standard deviation. In both cases, the empirical c.d.f.'s clearly approach such a Gaussian distribution as N increases. Though not shown, this result is also seen for $\rho=1$ as predicted by theory since ELS and LLS have the same asymptotic Gaussian lifetime behavior. According to ELS theory the lifetime is also asymptotically Gaussian for $\rho=0.75$, but only approximate arguments have been given to suggest that this also holds under LLS. For $\rho=0.5$, no theoretical proof exists to show that either ELS or LLS lifetime is indeed asymptotically Gaussian.

Figures 9–11 show the mean, standard deviation, and coefficient of variation of lifetime for $1/2<\rho<1$. For $\rho=1$, both ELS and LLS bundles have mean exactly one for all N and standard deviation decreasing as $1/\sqrt{N}$, as seen in the empirical plots. For $1/2<\rho<1$, LLS was argued earlier to have very similar behavior to ELS but with LLS producing slightly longer lifetimes. Under ELS the mean, standard deviation, and coefficient of variation were given, respectively, by Eqs. (3.3), (3.9) [based on Eq. (3.5)], and (3.10). Though not shown in Fig. 9, for $\rho=0.75$ the mean under LLS was found to be about 8% larger than under LLS. The standard deviation was found empirically to decrease for larger N (above 16 384) as $N^{-0.4709}$ with a regression coefficient of 0.999 85, which is very close to the $N^{-1/2}$ scaling behavior of ELS, though LLS values were consistently about 36% larger for each N. It is not entirely clear that the LLS exponent is indeed 1/2 when $\rho=0.75$, and finite size effects are likely only to affect the third decimal place. For $\rho=1/2$ the mean under ELS still follows Eq. (3.3) and thus has a large N limit of 2. Figure 9 shows that the LLS empirical mean is only slightly larger than 2 by perhaps 10%. On the other hand, by Eq. (3.9) [based on Eq. (3.6)] the ELS standard deviation is approximately $\sqrt{(\ln N)/(NL)}$, which is a departure from that for $\rho>1/2$. Under LLS, however, careful study of the empirical standard deviation for $N=16\,384-1\,048\,576$ shows that a power law with exponent 0.4042 provides a visibly much better data fit (regression coefficient 0.999 66) than does this ELS result. Using all data from $N=8$ upward also yields an excellent fit with exponent changed trivially to 0.3871. Thus a subtle but fundamental difference between ELS and LLS clearly emerges for the transition value $\rho=1/2$.

Figure 12 shows plots of empirical fiber failure times versus fraction of failed fibers in an LLS bundle of $N=4096$ fibers (solid lines) for $\rho=0.5$, 0.75, and 1. Also shown is the corresponding result, Eq. (3.4), from ELS theory (dotted lines). As expected ELS and LLS behavior are close to identical. These curves would remain unchanged for larger N. Figures 15 and 16, corresponding to $\rho=0.5$ and 0.75, respectively, show plots of the empirical fiber failure times in an actual LLS bundle of 4096 fibers (horizontal axis) against the times anticipated from ELS theory for the same fraction of failed fibers in a large bundle, Eq. (3.4). As more and more fibers fail, fiber failure times in LLS bundles become longer than those in ELS bundles by a modest amount, and the effect becomes more pronounced as ρ decreases from 1 down to 1/2. Not shown is the corresponding plot for $\rho=1$ which essentially is a straight line with slope one.

C. Bundle lifetime behavior for $0<\rho<1/2$

Figures 17 and 18 show two empirical plots of the c.d.f. for bundle lifetime, $G_N(t)$, versus standardized time t for the case $\rho=0.1$ and bundle sizes $N=8,16,32,64,\ldots,1\,048\,576$, each with 1024 replications. In Fig. 17 the lifetime data are normalized by subtracting out the respective sample means and dividing by the respective sample standard deviations and then plotted on Gaussian coordinates. Clearly the empirical c.d.f.'s do not approach a Gaussian distribution as N in-

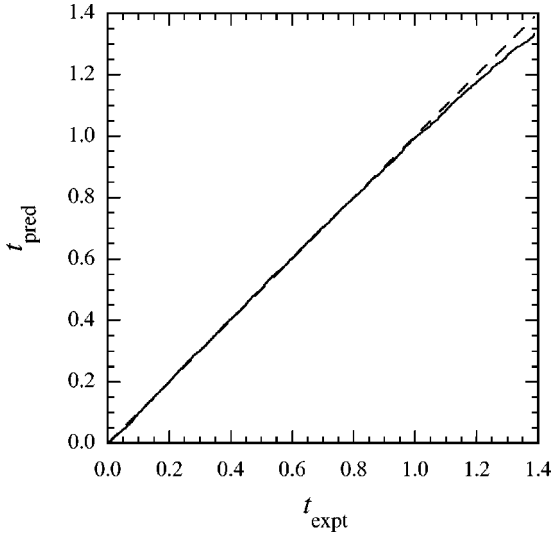

FIG. 16. Predicted t_{pred} versus empirical t_{expt} just as in Fig. 15 except $\rho=0.75$.

creases, unlike for $\rho>1/2$. In Fig. 18, the normalized lifetime data is plotted on the coordinates of the extreme value, double exponential form, Eq. (4.50), as motivated by the case $\rho=0$; that is $-\ln[-\ln G_N(t)]$ is plotted versus t. Remarkably the data yield a near straight line fit as N grows large. (Small upward bias in the extreme lower and upper tails results from our choice of vertical plotting positions i/N in graphing.) Although not shown, results for $\rho=0.25$ are nearly identical.

Figures 9–11 also show plots of the empirical mean, standard deviation, and coefficient of variation of lifetime as a function of N on log-log coordinates. The plots are based on 1024 replications each for $N=8,16,32,64,\ldots,1\,048\,576$. For $0<\rho<1/2$, the ELS mean again follows Eq. (3.3), and so has a large N limit $1/\rho$, though the deviation decays only as $N^{-\rho}$. The LLS empirical means for $\rho=0.25$ and 0.1 at N

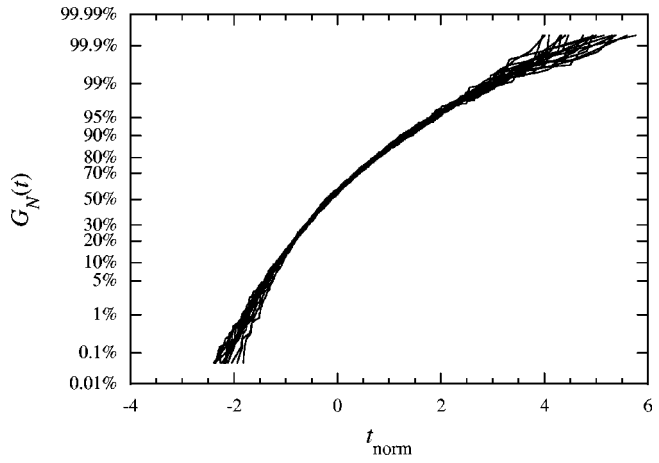

FIG. 17. Cumulative distribution function, $G_N(t)$, versus normalized bundle failure time, t_{norm} (actual time minus sample mean then divided by sample standard deviation) plotted on Gaussian coordinates for $\rho=0.1$ and LLS bundles with $N=8,16,32,64,\ldots,1\,048\,576$ fibers (1024 replications each).

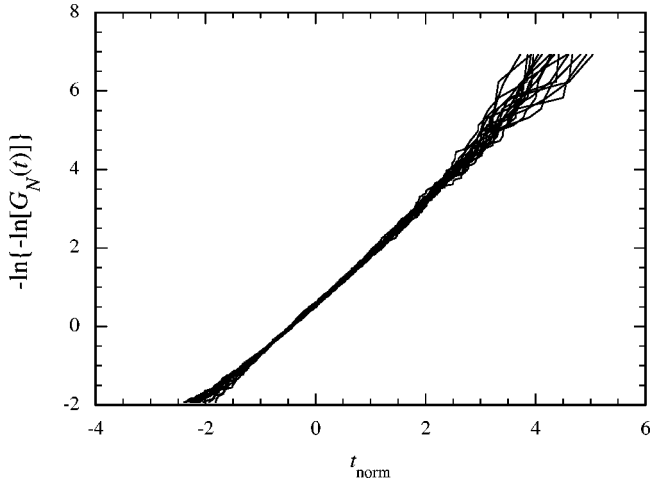

FIG. 18. $G_N(t)$ under the same conditions as in Fig. 17 except on coordinates of the extreme value, double exponential distribution.

$=1\,048\,576$ are about 4.1 and 7.9, which exceed the ELS values by roughly 5%. By Eq. (3.7) and Eq. (3.9) the ELS standard deviation scales for large bundles as $N^{-\rho}$. Power-law fits to the LLS data from $N=16\,384$–$1\,048\,576$ gave $1.7129N^{-0.250\,44}$ and $1.3872N^{-0.100\,31}$ so the exponents are almost identical to the exact ELS values -0.25 and -0.1, respectively. The LLS standard deviations, however, are about 20% and 11% higher than for ELS. For $\rho=0$, ELS and LLS are identical, and for larger N the mean grows as $\ln N$ and the standard deviation remains fixed of order one.

Figure 12 shows plots of empirical fiber failure times versus fraction of failed fibers in an LLS bundle of 1024 fibers (solid lines) and for $\rho=0.1$ and 0.25. Also shown is the result, Eq. (3.4), calculated from ELS theory (dotted lines). As expected, ELS and LLS behavior are close to identical and would remain so for even larger N. Figures 19 and 20, for $\rho=0.1$ and 0.25, respectively, show plots of the empirical

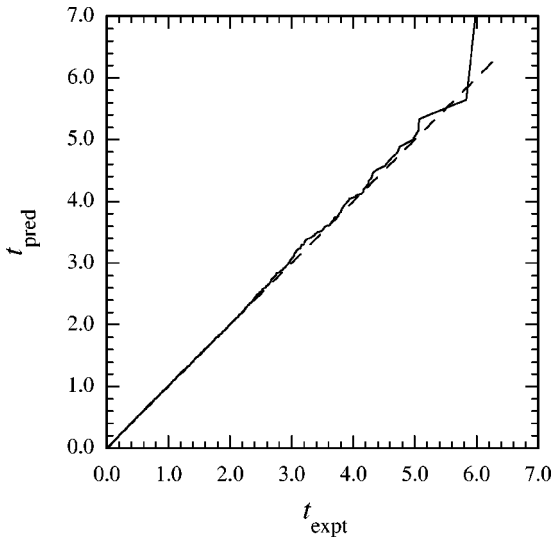

FIG. 19. Predicted t_{pred} versus empirical t_{expt} just as in Fig. 15 except $\rho=0.1$.

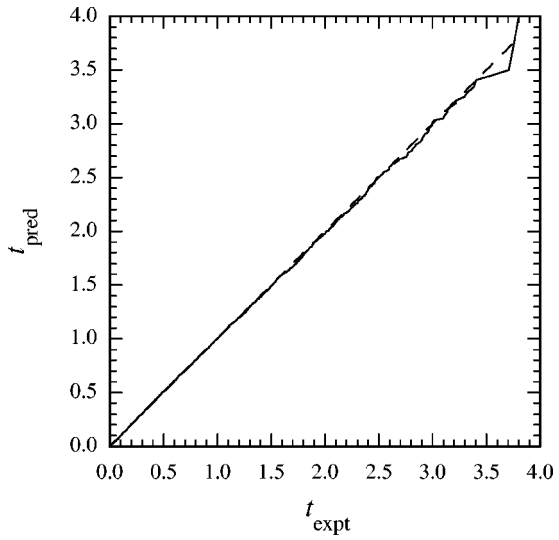

FIG. 20. Predicted t_{pred} versus empirical t_{expt} just as in Fig. 15 except $\rho=0.25$.

fiber failure times in an LLS bundle of 4096 fibers (horizontal axis) against the times anticipated from ELS theory, Eq. (3.4). For $\rho=0.25$, as more fibers fail, the LLS bundle failure times lag those under ELS by a modest amount, but less than for $\rho=1/2$. When $\rho=0$ the lagging appears to turn into leading, but this happens for this particular realization but not in general since the mean lifetime is greater under LLS, though the variability is somewhat larger (so such realizations are more common). Note that as ρ decreases, the last few fiber failures increasingly occupy a larger fraction of the overall lifetime, which results in breakdown of Gaussian lifetime behavior as the averaging effect in summing interfiber failure times is lost.

VI. DISCUSSION

The LLS model we have considered is virtually identical to that of Tierney [15,17] and Phoenix and Tierney [16]. We have assumed $\beta=1$, which has allowed some nonessential simplifications in the analysis and computations. These authors only considered the regime $\rho>1$, but we have investigated also the regimes $0<\rho\leqslant 1$. In Sec. IV, for the case $\rho>1$, where brittle cracklike behavior prevails we were able to develop explicit, closed-form approximations for the characteristic distribution function $W(t)$ and related quantities such as the critical cluster size k^* and the dependence of bundle lifetime on N. For $0<\rho\leqslant 1$ we also demonstrated that LLS is very close to ELS in behavior with similar scalings for the mean and standard deviation. In fact, $\rho=1$ was found to be a transition value where the bundle lifetime distributions are the same and Gaussian for large N (though with different spatial patterns of failures). While this Gaussian lifetime behavior appears to persist down to $\rho=1/2$, we demonstrated computationally that LLS and most likely ELS do not have Gaussian lifetime behavior for $0<\rho<1/2$, but have behavior related to the double-exponential, extreme-value distribution for the maximum of independent and identically distributed exponential random variables but with different, known forms for the mean and standard deviation.

Our model and some of the results also have close connection to the models of Gotlib *et al.* [37], and of Curtin and coworkers [39–42] for failure in a 2D lattice where failure clusters may wander somewhat in 2D. In their model, however, the stress concentrations around long linear clusters of breaks scaled as the square root of the cluster length rather than the length itself, thus introducing the exponent 1/2. (Their model also had longer range stress redistribution decreasing roughly as the $-1/2$ power of distance from the cluster tip.) As a result, our transition value $\rho=1$ is moved up to $\rho=2$, a value identified by Curtin and coworkers [41,42] who also report percolationlike failure for $\rho\leqslant 2$ but without the explicit mathematical connection to ELS that we have established for $\rho\leqslant 1$. Also, Curtin and coworkers did not obtain the power prefactor we have determined in our estimates of $W(t)$. This prefactor is important, and neglecting it may be responsible for some of the disagreement between their theory and simulation. Curtin and coworkers [41,42] also have discussed the difference between the time to development of a critical cluster versus the time to final failure, which includes the additional time the cluster takes to become catastrophic. They refer to this time difference as a rigid shift involving the factor $2/\rho$ whereas we find that it is primarily a scale factor in the lifetime distribution, in our case approximately $1-\pi^2/(6\rho)$ rather than $1-1/\rho$ as would occur following their approach. In our case the version based only on time to critical cluster formation actually behaves better in comparison to the simulation results.

The form of the lifetime distribution bears close resemblance to the form found in static strength as obtained in Phoenix and Beyerlein [22] and Wu and Leath [35]. In fact, upon applying an increasing load history, $\mathcal{L}(t)=\mathcal{B}t, t\geqslant 0$, and taking the bundle strength to be the load σ at the time of failure, it can be shown [16] that the distribution function for bundle strength is obtained from that for lifetime as $G_N\{\sigma^{\rho+1}/[\mathcal{B}(\rho+1)]\}$. (In fact, under power-law breakdown any positive applied bundle load history can be treated in a similar way.) Thus in Eq. (4.26), the exponent on σ becomes $(\rho+1)/(\rho-1)$ as compared to unity in the static model in Phoenix and Beyerlein [22]. They point out an apparent transition to ELS behavior for small values of the Weibull shape parameter $\hat{\rho}$ for fiber strength, which corresponds to $\rho+1$ in the present case. Thus the current transition at $\rho=1$ corresponds to $\hat{\rho}=2$. This transition is more explicit in the present case because of the appearance of $1/(\rho-1)$ in the exponent on time or stress. It holds for all volumes, whereas in the strength case, reverting to LLS-like scaling may eventually occur for large enough volumes. This difference in the hardness of the transition to ELS behavior between strength and lifetime requires more study.

We conclude that the lifetime distribution is much more sensitive to the form of the localized fiber stress redistribution mechanism for ρ larger than a critical value, ρ_c, than below it, and that there will be a drastic change in behavior through the transition. This critical value is expected to vary with β, when the model is extended to permit values of β other than unity, as we have assumed.

Finally, we note again the importance of blending physical theory with computational methodology in order to identify and verify the scalings that emerge.

ACKNOWLEDGMENTS

We thank Leon Knopoff for motivating us to study the problem and providing insights connecting the work to the literature on modeling earthquakes. We wish to thank Kirby Baker and Richard Korf for valuable comments regarding this algorithm and recent developments in the computer science literature. During the latter part of this project, W.I.N. was the Belkin Visiting Professor in the Department of Computer Science and Applied Mathematics of the Weizmann Institute of Science, and gratefully acknowledges its support. S.L.P. acknowledges financial support form the National Science Foundation (CMS-9800413) and from the National Institute of Standards and Technology (PO No. 43SBN867130).

APPENDIX: MERGE-SORT ALGORITHM FOR MEGAFIBER BUNDLE SIMULATION

As mentioned, several investigations of time-dependent fiber bundle or network behavior under localized load sharing have been reported in the literature. Their associated simulations were limited typically to $\approx 10^3$–10^4 fibers and approximations were often introduced to reduce the computational burden. While computer CPU speeds have since increased by an order of magnitude, present day computers remain incapable of significantly expanding the computational size to that required to better understand the scaling features of the underlying physical problem. The LLS rule we have used simplifies the analysis, but computational obstacles remain.

At the outset, we believed that a wholesale reconstruction of the computational algorithms had the potential to dramatically improve our ability to undertake very large simulations. When an individual fiber fails, the computational cost of calculating the remaining lifetimes of its nearest neighbors is very small, and requires $\mathcal{O}(N)$ operation counts for the entire system of N fibers. The overwhelming expense has resulted from two tasks: The first is to identify the nearest surviving neighbors onto which the load of the failed fiber must be placed; the second is to establish which of all the remaining survivors will be the next to fail. Each of these tasks can be shown to require $\mathcal{O}(N^2)$ operations. Thus to proceed from simulations describing thousands of fibers to simulations describing millions, a millionfold increase in the operation count was anticipated. Using data management concepts from computer science we now show how the first task can be reduced to one requiring only $\mathcal{O}(N)$ operations and the second to one requiring $\mathcal{O}(N \ln N)$.

From a physical standpoint, at any given dimensionless time t we can describe our array of fibers by three state variables per fiber. First, we know the status of the ith fiber in terms of the state S_i, which is 0, if it is broken, and 1, if it is intact.

Second, we know the current load ℓ_i applied to that fiber, if intact. Third, we know the time t_i when that fiber is projected to fail, assuming that its load does not change. Should the load applied to the ith element change to ℓ_i' at time t due to failure of a neighbor, we have a rule $\mathcal{R}$ for calculating a revised projected lifetime t_i', namely $t_i' = t + \mathcal{R}(t_i - t, \ell_i, \ell_i')$, which replaces the previous value. In the power-law scheme, this rule has the form of a contraction mapping

$$t_i' = t + (t_i - t)\left(\frac{\ell_i}{\ell_i'}\right)^{\rho}. \tag{A1}$$

Apart from the LLS rule, this equation describes the only ''physics'' in the problem.

Turning to the data management issues of the two tasks above, we assume that the N fibers, indexed from left to right by $i = 1,2,\ldots,N$ have initial lifetimes t_i, which are individual independent deviates (i.i.d.) assigned from some well-defined distribution function, in the present case the Weibull distribution, Eq. (2.8), with $\beta = 1$ and $L = 1$. Moreover, we assume that their initial loads ℓ_i have been assigned, in the present case uniformly with value $L = 1$. We assume that their respective states S_i are unity. For reasons encountered shortly, it is advantageous to employ fiber bundles whose size is an integral power of 2, i.e., $N = 2^n$, where n is an integer. (This can be circumvented through a scheme of adding fictitious failed fibers with benign load-sharing influence.)

We assume that when an interior surviving fiber fails, its load is redistributed equally onto its nearest surviving neighbors, one on its left and one on its right. When a boundary surviving fiber fails it transfers all its load to the nearest interior survivor. See Sec. II A for complete details. (Other boundary schemes, such as periodic boundary conditions, are an easy adaptation.) The immediate problem is to find these nearest surviving neighbors using the fewest possible operations.

Next we create two integer arrays whose N elements are pointers associated with the N fibers. For convenience, we refer to these as forward and backward pointers, f_i and b_i. We also define functions based on these pointers, i.e.,

$$f(i) = f_i \quad \text{and} \quad b(i) = b_i. \tag{A2}$$

Simply stated, for the ith fiber, f_i identifies its nearest surviving neighbor in the forward (or right) direction, and b_i identifies its nearest surviving neighbor in the backward (or left) direction. To locate the boundary or terminal survivors (whose load sharing rule differs from interior survivors) we introduce a ''flag.'' For the left and right terminal survivors, we set $b_i = 0$ and $f_i = 0$, respectively. This indexing scheme is illustrated in Fig. 21. Initially, for all interior fibers for whom $S_i \neq 0$, we set $f_i = i + 1$ and $b_i = i - 1$.

For the mth fiber, if it is an interior survivor the associated entries in the up-to-date pointer arrays identify its right and left nearest survivors as $f(m)$ and $b(m)$, respectively. When the mth fiber fails, we need to modify the stored pointers associated with these survivors $f(m)$ and $b(m)$. The forward pointer for fiber $b(m)$ must become $f(m)$ (rather than

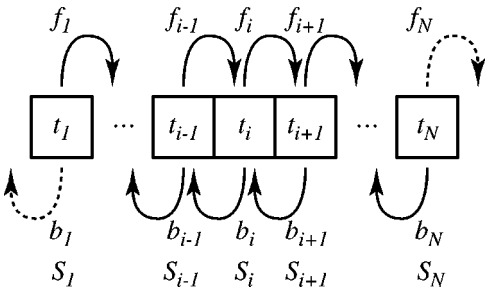

FIG. 21. Pointer arrays employed in identification of survivors.

m) and the backward pointer for fiber $f(m)$ must become $b(m)$ (rather than m). Thus we make the assignments,

$$f[b(m)]=f(m),$$

$$b[f(m)]=b(m). \tag{A3}$$

For terminal survivors, if fiber m was the left-most surviving fiber, then we set

$$b[f(m)]=0, \tag{A4}$$

and if it was the right-most survivor we set

$$f[b(m)]=0. \tag{A5}$$

In so doing, element m is effectively eliminated from all future computations, and of course, S_m is set to zero. Thus by simply updating these two pointer arrays as fibers fail, we have essentially eliminated the task of finding the nearest survivors and this task has been relegated to $\mathcal{O}(N)$. We can also update the loads on these surviving fibers and use the contraction mapping, Eq. (A1), to revise their projected lifetimes. Our system of pointer arrays is closely related to what is called a ''doubly linked list'' (see Cormen *et al.* [56]) in the computer science literature. (This scheme can be expanded to consider more distant surviving neighbors under more general local load-sharing rules.)

We now turn our attention to finding the next fiber among the survivors to fail. Scanning the entire array would take $\mathcal{O}(N)$ operations, which must be performed as each of the N fibers fails, making this part of the problem $\mathcal{O}(N^2)$. We now show how to avoid the scan and to identify the next fiber to fail in only $\mathcal{O}(\log_2 N)$ operations. This is closely related to the task of finding a telephone number in a telephone directory whose N elements are already alphabetically ordered. A sequential search would take $\mathcal{O}(N)$ operations. A better approach is to ''divide and conquer'' where a hierarchy of simpler problems is solved. In the telephone number analogy, we first ask: ''Is the number in the first half of the telephone book?'' If the answer initially is yes, we henceforth ignore the second half and repeat the question. We find our number in $\mathcal{O}(\log_2 N)$ operations.

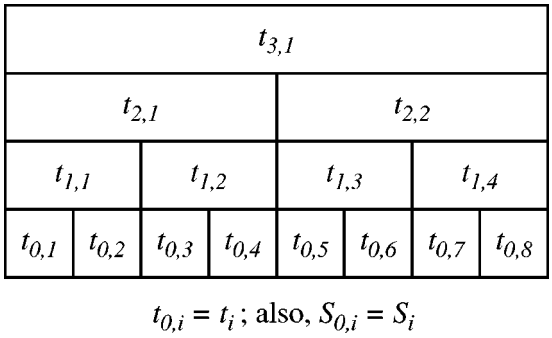

FIG. 22. Hierarchical structure employed in identification of prioritization of failures.

The preceding discussion illustrates that most of the $\mathcal{O}(N^2)$ pairwise operations are redundant once we have some information available as to the order of subsets of the complete set of fibers. The avoidance of redundant computations and making algorithms ''computationally irreducible'' is widely employed in other disciplines. For example, the Cooley–Tukey fast Fourier transform algorithm applied to data sets with N elements reduces the otherwise $\mathcal{O}(N^2)$ operation task of performing a Fourier transform to $\mathcal{O}(N \ln N)$ operations. Newman and Gabrielov [45] explored a hierarchically organized set of fiber bundles, reducing $\mathcal{O}(2^N)$ operations to $\mathcal{O}(N^2)$ operations, where N was the number of levels in the hierarchy. Newman *et al.* [46–49] also developed computationally irreducible algorithms in applications to fiber bundle problems.

The class of computer science algorithms for ranking (by some criterion, such as failure times) of a list is often called a ''sort-merge'' algorithm, and it can be adapted to situations where the criterion is constantly being updated, but where other information is available. So-called ''heap-sort'' methods are theoretically more efficient for relatively uniformly distributed random data, but become less efficient and advantageous if substantial clustering in the data occurs. The scheme we describe below is not particularly efficient in terms of memory-utilization, but is simpler to program and more intuitive than memory-optimized dynamic sort-merge algorithms. Cormen *et al.* [56] offers an encyclopedic contemporary view of sorting and search algorithms.

We consider establishing a hierarchical tableau as shown in Fig. 22. It is also worthwhile visualizing this as a binary tree where each element in the tableau can be regarded as a node connecting ''parents'' to ''children'' and where children at the same level in the hierarchy of a given parent (or grandparent, etc.) are regarded as ''siblings.'' The lowest or ''0'' level of the tree corresponds with the original projected failure times (calculated as though the fiber loads, ℓ_i, remain as their initial values $L=1$), now designated via

$$t_{0,i}=t_i, \quad i=1,\ldots,N, \tag{A6}$$

with a similar tableau established to store the state variable information S_i.

Each pair of elements at the bottom of this tree come together to form a new node. For example, assuming that i is odd, we construct from $t_{0,i}$ and $t_{0,i+1}$ a node

$$t_{1,(i+1)/2} \equiv \min(t_{0,i}, t_{0,i+1}). \tag{A7}$$

(In this expression and in what follows, we will assume that the quotient of two integers preserves only the integer part.) Similarly, we find for the state tableau that

$$S_{1,(i+1)/2} \equiv S_{0,i} + S_{0,i+1} - S_{0,i} \times S_{0,i+1}, \tag{A8}$$

implying that a parent of the two children is intact if at least one of the subordinate elements is intact. The two preceding equations, that take us from level 0 to level 1, can also be used to take us from level p to level $p+1$, where $p = 0,1,\ldots,\log_2 N$. Thus $t_{p,i}$ and $S_{p,i}$ describe the elements within the range $1+2^{p-1}i$ to $2^p i$; $S_{p,i}$ is one only if at least one fiber in the subset is still intact while $t_{p,i}$ describes the earliest time to failure in that subset. It is also useful, at a modest increase in memory utilization, to store additional information at each node as we ascend the tree. For example, it is useful to know which element i at the lowest level corresponds to the position of the fiber with the earliest failure time contained within that range of elements. (In fact, if we store only that index information as a pointer array, we avoid the need to store the $t_{p,i}$ tableau, thereby saving significant memory with a barely noticeable increase in execution time.) We achieve this by constructing an additional binary tree $M_{p,i}$ paralleling the role of the tree $t_{p,i}$. While $t_{p,i}$ identifies the time for the first failure associated with the 2^p elements on that branch, $M_{p,i}$ identifies its corresponding location. All of the above is readily established by induction.

The initial setting up of the tableaus requires $\mathcal{O}(N)$ operations, which is essentially the same as the number of operations required to identify the most shortlived fiber. However, once set up, the tableaus eliminate the need to scan the list of surviving fibers, and operationally we need only go up the tree employing $\mathcal{O}(\ln N)$ operations instead of across it in $\mathcal{O}(N)$ operations. To understand this, consider what must be done when the mth fiber has its projected lifetime reduced, through load redistribution, or when it fails. Then, the fibers designated $2\times[(m+1)/2]-1$ and $2\times[(m+1)/2]$ correspond with the original fiber and its sibling in the tree. We now compute the lifetime and state of the parent of this pair, namely $t_{1,(m+1)/2}$ and $S_{1,(m+1)/2}$. (We should also store at this level of the hierarchy, as observed earlier, the location of the surviving fiber, if any, in $M_{1,(m+1)/2}$ contained in the original pair.) Here, we have updated the status of two children in order to obtain the status of their parent; this process can be repeated solely by moving up the tree-tableau by working along its branches instead of across its branches at the lowest level. The other branches in the tree remain unaffected.

We note that when a fiber fails, we may not need to go completely up all branches of the tree. To see why, we recall that we had previously identified that particular fiber as being the next to fail and, therefore, all of the timing, state variable, and position information stored in the tableaus are based on its imminent failure. However, when the projected times to failure of its nearest neighbors are reduced, there generally is a low probability that either of these neighbors will become the next fiber to fail. Thus it is highly advantageous to make the implementation of this algorithm aware of the possibility that the updating of the tableaus need not continue all the way to the top. Eliminating such unnecessary operations is analogous to ''asynchronous'' schemes encountered in computer science and makes this implementation of the search algorithm competitive with standard implementations of sort-merge algorithms (Cormen *et al.* [56]).

While simple in principle, our algorithm demands substantial care in developing its relatively complex logic. However, in execution, this logic requires remarkably little computational overhead. The theoretical speed enhancement of $\mathcal{O}(N/\log_2 N)$ is directly realized, losing only a factor of several in its achievement. For our ''megafiber'' or $2^{20} = 1\,048\,576$ fiber simulation, we could execute a single realization in less than a minute, which otherwise would have required several weeks. Ten-thousand realizations required several days, in contrast to an estimated century-long run. The algorithms presented here made it possible to explore large fiber bundle sizes over large numbers of realizations, as desired.

[1] H.E. Daniels, Proc. R. Soc. London, Ser. A **183**, 405 (1945).
[2] D.E. Gücer and J. Gurland, J. Mech. Phys. Solids **10**, 365 (1962).
[3] R.L. Smith and S.L. Phoenix, ASME J. Appl. Mech. **48**, 75 (1981).
[4] R.L. Smith, Ann. Prob. **10**, 137 (1982).
[5] B.D. Coleman, J. Appl. Phys. **27**, 862 (1956).
[6] B.D. Coleman, Trans. Soc. Rheol. **1**, 153 (1957).
[7] B.D. Coleman, Trans. Soc. Rheol. **2**, 195 (1958).
[8] S.L. Phoenix, SIAM (Soc. Ind. Appl. Math.) J. Appl. Math. **34**, 227 (1978).
[9] S.L. Phoenix, Adv. Appl. Probab. **11**, 153 (1979).
[10] D.G. Harlow and S.L. Phoenix, J. Compos. Mater. **12**, 195 (1978).
[11] D.G. Harlow and S.L. Phoenix, J. Compos. Mater. **12**, 314 (1978).
[12] R.L. Smith, Proc. R. Soc. London, Ser. A **372**, 539 (1980).
[13] C.-C. Kuo, Ph.D. thesis, Cornell University, 1983.
[14] C.-C. Kuo and S.L. Phoenix, J. Appl. Probab. **24**, 137 (1987).
[15] L. Tierney, Adv. Appl. Probab. **14**, 95 (1982).
[16] S.L. Phoenix and L.-J. Tierney, Eng. Fract. Mech. **18**, 193 (1983).
[17] L. Tierney, Stochastic Process. Appl. **18**, 139 (1984).
[18] W. Weibull, ASME J. Appl. Mech. **18**, 293 (1951).
[19] J. M. Hedgepeth, NASA TN D-882, 1961 (unpublished).
[20] F. Hikami and T.W. Chou, AIAA J. **28**, 499 (1990).
[21] I.J. Beyerlein, S.L. Phoenix, and A.M. Sastry, Int. J. Solids Struct. **33**, 2543 (1996).

[22] S.L. Phoenix and I.J. Beyerlein, in *Comprehensive Composite Materials*, edited by A. Kelly and C. Zweben (Pergamon-Elsevier Science, New York, 2000) Vol. 1, Chap. 1.19.
[23] L. de Arcangelis, S. Redner, and H.J. Herrmann, J. Phys. (France) Lett. **46**, L585 (1985).
[24] P.M. Duxbury, P.L. Leath, and P.D. Beale, Phys. Rev. B **36**, 367 (1987).
[25] P.M. Duxbury and P.L. Leath, J. Phys. A **20**, L411 (1987).
[26] *Statistical Models for the Fracture of Disordered Media*, edited by H. J. Herrmann and S. Roux (North-Holland, Amsterdam, 1990).
[27] H.M. Taylor and D.E. Sweitzer, Adv. Appl. Probab. **30**, 342 (1998).
[28] A. Hansen, in *Statistical Models for the Fracture of Disordered Media*, edited by H.J. Herrmann and S. Roux (North-Holland, Amsterdam, 1990).
[29] A. Hansen, E.L. Hinrichsen, and S. Roux, Phys. Rev. B **43**, 665 (1991).
[30] D.G. Harlow and S.L. Phoenix, J. Mech. Phys. Solids **39**, 173 (1991).
[31] P.L. Leath and P.M. Duxbury, Phys. Rev. B **49**, 14 905 (1994).
[32] S.D. Zhang and E.J. Ding, Phys. Lett. A **193**, 425 (1994).
[33] S.D. Zhang and E.J. Ding, Phys. Rev. B **53**, 646 (1996).
[34] M. Kloster, A. Hansen, and P.C. Hemmer, Phys. Rev. E **56**, 2615 (1997).
[35] B.Q. Wu and P.L. Leath, Phys. Rev. B **61**, 15 028 (2000).
[36] B.Q. Wu and P.L. Leath, Phys. Rev. B **62**, 9338 (2000).
[37] Y.Y. Gotlib, A.V. Dobrodumov, A.M. El'yashevich, and Y.E. Svetlov, Sov. Phys. Solid State **15**, 555 (1973).
[38] Y.Y. Gotlib, A.M. El'yashevich, and Y.E. Svetlov, Sov. Phys. Solid State **14**, 2672 (1973).
[39] W.A. Curtin and H. Scher, Phys. Rev. Lett. **67**, 2457 (1992).
[40] W.A. Curtin and H. Scher, Phys. Rev. B **45**, 2620 (1992).
[41] W.A. Curtin and H. Scher, Phys. Rev. B **55**, 12 038 (1997).
[42] W.A. Curtin, W. Pamel, and H. Scher, Phys. Rev. B **55**, 12 051 (1997).
[43] A. Hansen, S. Roux, and E.L. Hinrichsen, Europhys. Lett. **13**, 517 (1990).
[44] S. Roux, A. Hansen, and E.L. Hinrichsen, Phys. Rev. Lett. **70**, 100 (1993).
[45] W.I. Newman and A.M. Gabrielov, Int. J. Fract. **50**, 1 (1991).
[46] W.I. Newman, A.M. Gabrielov, T.A. Durand, S.L. Phoenix, and D.L. Turcotte, Physica D **77**, 200 (1994).
[47] W.I. Newman, A.M. Gabrielov, S.L. Phoenix, and D.L. Turcotte, in *Spatio-Temporal Patterns in Nonequilibrium Complex Systems*: *NATO Advanced Research Workshop* edited by P.E. Cladis and P. Palffy-Mulhoray (Addison-Wesley, Reading, MA, 1995).
[48] W.I. Newman, D.L. Turcotte, and A. Gabrielov, in *Reduction and Predictability of Natural Disasters*: *Santa Fé Institute Studies in the Sciences of Complexity*, edited by J.B. Rundle, W. Klein, and D.L. Turcotte (Addison-Wesley, Reading, MA, 1995), Vol. 25.
[49] W.I. Newman, D.L. Turcotte, and A. Gabrielov, Phys. Rev. E **52**, 4827 (1995).
[50] T. Yamashita and L. Knopoff, Geophys. J. R. Astron. Soc. **96**, 389 (1989).
[51] B.K. Atkinson, J. Geophys. Res. **89**, 4077 (1984).
[52] D.T. Griggs, Bull. Geol. Soc. Am. **51**, 1001 (1940).
[53] R. P. Kelley, Ph.D. thesis, Cornell University, 1978.
[54] E. Yaschin, Doctoral dissertation, Technion, Haifa, Israel, 1981.
[55] P.D. Feigin and E. Yaschin, J. Appl. Probab. **19**, 500 (1982).
[56] T.H. Cormen, C.E. Leiserson, and R.L. Rivest, *Introduction to Algorithms* (MIT Press, Cambridge, MA, 1990).